AGU PUBLICATIONS

JGR

Journal of Geophysical Research: Space Physics

RESEARCH ARTICLE
10.1002/2015JA022281

Key Points:
- Global ionosphere of Mars response to the solar cycle is investigated with multiple data sets
- Empirical modeling of the neutral scale height with solar cycle
- Temperature and pressure balance analysis with solar cycle

Correspondence to:
B. Sánchez-Cano,
bscmdr1@leicester.ac.uk

Citation:
Sánchez-Cano, B., et al. (2016), Solar cycle variations in the ionosphere of Mars as seen by multiple Mars Express data sets, *J. Geophys. Res. Space Physics*, *121*, 2547–2568, doi:10.1002/2015JA022281.

Received 17 DEC 2015
Accepted 12 FEB 2016
Accepted article online 22 FEB 2016
Published online 8 MAR 2016

Solar cycle variations in the ionosphere of Mars as seen by multiple Mars Express data sets

B. Sánchez-Cano[1], M. Lester[1], O. Witasse[2], S. E. Milan[1], B. E. S. Hall[1], M. Cartacci[3], K. Peter[4], D. D. Morgan[5], P.-L. Blelly[6], S. Radicella[7], A. Cicchetti[3], R. Noschese[3], R. Orosei[8], and M. Pätzold[4]

[1]Radio and Space Plasma Physics Group, Department of Physics and Astronomy, University of Leicester, Leicester, UK, [2]ESTEC-Scientific Support Office, European Space Agency, Noordwijk, Netherlands, [3]Istituto Nazionale di Astrofisica (INAF), Istituto di Astrofisica e Planetologia Spaziali (IAPS), Rome, Italy, [4]Rheinisches Institut für Umweltforschung an der Universität zu Köln, Köln, Germany, [5]Department of Physics and Astronomy, University of Iowa, Iowa City, Iowa, USA, [6]Institut de Recherche en Astrophysique et Planétologie, Toulouse, France, [7]Telecommunications/ICT for Development Laboratory, Abdus Salam International Centre for Theoretical Physics (ICTP), Trieste, Italy, [8]Istituto di Radioastronomia, Istituto Nazionale di Astrofisica, Bologna, Italy

Abstract The response of the Martian ionosphere to solar activity is analyzed by taking into account variations in a range of parameters during four phases of the solar cycle throughout 2005–2012. Multiple Mars Express data sets have been used (such as Mars Advanced Radar for Subsurface and Ionospheric Sounding (MARSIS) in Active Ionospheric Sounding, MARSIS subsurface, and MaRS Radio Science), which currently cover more than 10 years of solar activity. The topside of the main ionospheric layer behavior is empirically modeled through the neutral scale height parameter, which describes the density distribution in altitude, and can be used as a dynamic monitor of the solar wind-Martian plasma interaction, as well as of the medium's temperature. The main peak, the total electron content, and the relationship between the solar wind dynamic pressure and the maximum thermal pressure of the ionosphere with the solar cycle are assessed. We conclude that the neutral scale height was different in each phase of the solar cycle, having a large variation with solar zenith angle during the moderate-ascending and high phases, while there is almost no variation during the moderate-descending and low phases. Between end-2007 and end-2009, an almost permanent absence of secondary layer resulted because of the low level of solar X-rays. Also, the ionosphere was more likely to be found in a more continuously magnetized state. The induced magnetic field from the solar wind, even if weak, could be strong enough to penetrate more than at other solar cycle phases.

1. Introduction

The dayside ionosphere of Mars consists mainly of two layers. In general terms, the peak of the main layer is located between 125 and 140 km altitude with a typical electron density variation of $0.4–2 \cdot 10^{11}$ el/m^3 depending on solar zenith angle and solar activity [e.g., *Whitten and Colin*, 1974; *Gurnett et al.*, 2005; *Witasse et al.*, 2008; *Peter et al.*, 2014] and is primarily produced by solar extreme ultraviolet (EUV) photons [e.g., *Schunk and Nagy*, 2009]. A secondary layer with a peak located at around 110–115 km altitude is formed mainly by soft X-ray solar photons with a significant contribution to the ionization due to secondary electrons and photoelectrons [e.g., *Schunk and Nagy*, 2009]. This layer is considerably weaker than the main peak and is not always formed, but when present, it is not negligible since it can contribute up to about 10% of the total electron content (TEC) [*Sánchez-Cano et al.*, 2015a]. Because the plasma is in hydrostatic equilibrium up to 170–200 km of altitude [e.g., *Schunk and Nagy*, 2009], photochemical processes control the behavior of the two main global ionospheric layers. In this photochemical region, the Martian ionosphere is well represented, at least to first order, by an α-Chapman-type layer [e.g., *Gurnett et al.*, 2005; *Withers*, 2009; *Sánchez-Cano et al.*, 2013].

Since the Sun is the main source of ionization, any variation in the solar radiation produces large dynamics in the electron density, both in time and in space. Examples include the solar cycle, solar flares, seasons, or the diurnal variation [e.g., *Bougher et al.*, 2015a; *Sánchez-Cano et al.*, 2015b; *Mendillo et al.*, 2006; *González-Galindo et al.*, 2013; *Zou et al.*, 2011]. Planetary surface phenomena like dust storms, thermal atmospheric tides, crustal magnetic fields, or the topography itself can also contribute to changes in ionospheric structures [e.g., *Withers and Pratt*, 2013; *Withers et al.*, 2003; *Matta et al.*, 2015; *Wang and Nielsen*, 2004]. Several examples of the ionospheric variability from Mars Express radio occultation profiles are shown in *Withers et al.* [2012a, 2012b]. Other factors such as the presence of an induced magnetic field can produce a compression at the top of

the ionosphere [*Shinagawa and Cravens*, 1989; *Witasse*, 2000; *Morel et al.*, 2004; *Sánchez-Cano et al.*, 2015b]. However, the solar cycle is the feature which can play one of the most important long-term roles in ionospheric variability [*Withers et al.*, 2014; *Bougher et al.*, 2015a; *Sánchez-Cano et al.*, 2015b]. Variations in EUV flux during the different phases of the solar cycle produce changes in the neutral atmosphere and, as a consequence, also in the ionospheric temperatures and densities. Additionally, the solar wind is different for each phase of the solar cycle, such as the interplanetary magnetic field (IMF) or the velocity of the solar wind [e.g., *Imber et al.*, 2013]. This produces variations in the transport and ionization rates in the ionosphere. These factors combine to form a complex environment that modulates the Martian ionospheric environment by creating different couplings between the neutral atmosphere and the ionosphere, induced magnetic fields at lower altitudes, etc.

The recent work of *Sánchez-Cano et al.* [2015b] showed that at least for a narrow range of solar zenith angle (χ, SZA), there was a clear difference in behavior of the Martian ionosphere during the solar cycle, and in particular during the recent extended low solar activity phase, where a large density reduction in the topside was found. The objective of this paper is to extend that work to broader solar zenith angle and altitude ranges by taking into account the different phases of the solar cycle and multiple Mars Express data sets. In this context, the general response of the Martian ionosphere to the solar activity is empirically modeled. This study includes assessment of the following. (1) The behavior of the topside main layer is analyzed through the neutral scale height parameter. (2) Variations in the peak characteristics of the main layer are assessed. (3) A possible anomalous behavior of the secondary layer for the extreme solar minimum phase between end-2007 to end-2009 is examined. (4) The daily TEC variation during the solar cycle is evaluated, as well as compared with the empirical modeling. (5) As a by-product, the daily neutral and plasma temperatures at the main peak altitude are obtained. Finally, (6) an estimation of the solar wind-ionosphere interaction along the solar cycle is presented by considering the relationship between the dynamic pressure of the solar wind and the maximum ionospheric thermal pressure.

2. Data Set

Figure 1 shows various parameters describing the solar output in the first 10 years of the Mars Express mission at Mars: the sunspot number (SSN) in the first panel, the EUV solar irradiance measured by Thermosphere, Ionosphere, Mesosphere Energetics and Dynamics (TIMED)-Solar EUV Experiment (SEE) satellite at a wavelength of 30.5 nm at 1 AU in the second panel, the EUV solar irradiance at 30.5 nm scaled to the Mars heliocentric distance in the third panel, and the X-ray background radiation measured by the GOES family of satellites extrapolated to the Mars location in the fourth panel. The EUV solar irradiance of 30.5 nm has been selected as the most representative wavelength able to ionize the Martian ionosphere since it is the closest wavelength measured by TIMED to the Helium 30.4 nm intense line of the spectrum, which causes the major ionization of the CO_2 molecule in the Martian atmosphere [*Frahm et al.*, 2006]. Nevertheless, we note that wavelengths from 1 to 90 nm could play an additional notable role in the CO_2 ionization [*Girazian and Withers*, 2013]. In order to investigate the ionospheric response to solar cycle changes, following exactly the same criteria as *Sánchez-Cano et al.* [2015b], four periods in the solar cycle were created according to notable changes in the four parameters of Figure 1 altogether.

1. *Period A*. From the Mars Express MARSIS radar (described later) deployment in mid-June 2005 until mid-September 2007. This period was characterized by moderate solar activity in the declining phase of solar cycle 23. The level of EUV 30.5 nm irradiance at Mars was between $1.2 \cdot 10^{-4}$ and $1.9 \cdot 10^{-4}$ W/m^2, while the X-ray flux at Mars was larger than 10^{-7} W/m^2 at the very beginning of the period and then always lower than 10^{-7} W/m^2.
2. *Period B*. From mid-September 2007 to mid-September 2009. This period corresponds to the low solar activity phase of solar cycle 23/24, which was particularly low and longer than in previous solar minima [e.g., *Solomon et al.*, 2010]. The level of EUV 30.5 nm irradiance at Mars was lower than the minimum of period A during most of 2008 ($1.0–1.2 \cdot 10^{-4}$ W/m^2) while reaching similar levels to period A for the rest of the phase ($1.2–1.6 \cdot 10^{-4}$ W/m^2). The variation is a consequence of the planet's orbital distance from the Sun. Moreover, the whole period is characterized by a notable reduction in the X-ray flux background at Mars, which was lower than 10^{-8} W/m^2 (i.e., lower than the solar X-ray catalog threshold).
3. *Period C*. From mid-September 2009 to mid-February 2011. This period was characterized by moderate solar activity (same flux level as in period A) but during the ascending phase of the solar cycle 24. This period is the shortest of the four intervals. The main change from period B is a notable increment of X-ray flux, which reached the same level as in period A.

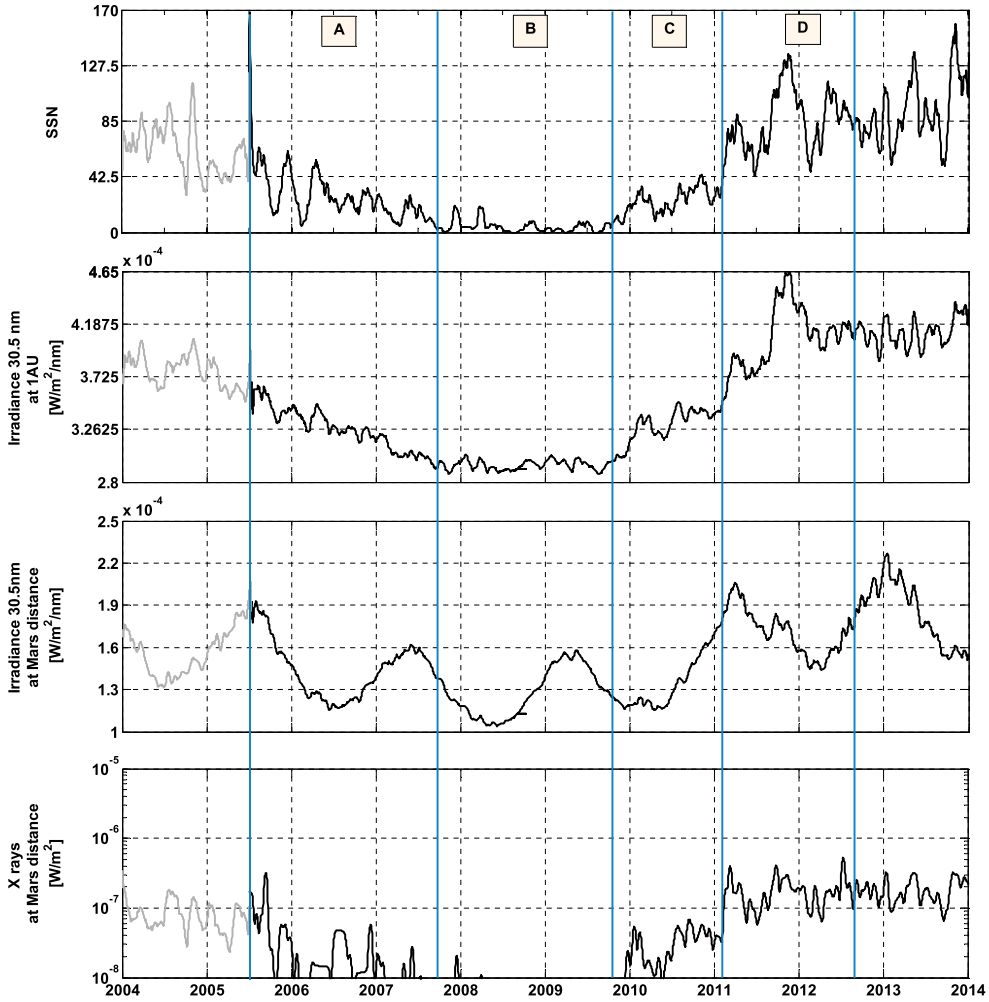

Figure 1. Solar cycle evolution from the arrival time of Mars Express until 2014. (first panel) solar sun spot number (SSN). (second panel) EUV solar irradiance at a wavelength of 30.5 nm (from TIMED-SEE satellite at 1 AU). (third panel) EUV solar irradiance at 30.5 nm scaled to Mars distance. (fourth panel) Solar X-rays measured by GOES family satellites scaled to Mars distance.

4. *Period D*. From mid-February 2011 to June 2012. This period corresponds to the high solar activity phase of solar cycle 24, where the average values of EUV and X-ray fluxes were clearly higher than in the former interval (period C), $1.4 \cdot 10^{-4}$ – $2.2 \cdot 10^{-4}$ W/m^2 of EUV 30.5 nm irradiance at Mars and an average of $5 \cdot 10^{-7}$ W/m^2 of X-ray flux.

In order to assess the impact of the variation of the EUV spectrum at Mars as a result of the planetary orbital distance, *Sánchez-Cano et al.* [2015b] showed that for a narrow solar zenith angle interval, the Martian topside TEC behavior of the main layer as a function of the EUV solar irradiance at 30.5 nm at Mars was different depending on the solar cycle phases. Particularly, TEC did not indicate any significant dependence on the EUV flux during the low solar activity phase, while during the other three periods, TEC showed an ascending linear trend with EUV flux. This indicated that the Martian ionospheric behavior, for the same level of solar activity (see, e.g., Figure 1, third panel), is different depending on the solar cycle phases, especially for the low solar activity phase.

The Mars Advanced Radar for Subsurface and Ionospheric Sounding (MARSIS) [*Picardi et al.*, 2004] onboard Mars Express spacecraft [*Chicarro et al.*, 2004] has been probing the ionosphere of Mars since mid-June 2005 [*Orosei et al.*, 2014]. This instrument has two different operational modes, from which different ionospheric parameters can be obtained. In the Active Ionospheric Sounding (AIS) mode [*Gurnett et al.*, 2005], MARSIS works as a topside ionospheric sounder, providing the vertical electron density profile of the topside ionosphere as a data product

[*Sánchez-Cano et al.*, 2012; *Morgan et al.*, 2013]. In the subsurface mode [*Gurnett et al.*, 2005], MARSIS works as a geophysical radar to analyze the subsurface of the planet, and from this, the TEC of the entire atmosphere can be retrieved as a by-product [*Safaeinili et al.*, 2007; *Mouginot et al.*, 2008; *Cartacci et al.*, 2013].

To investigate the solar zenith angle-dependent ionospheric response to solar cycle variations, this study has analyzed a total of 2814 AIS topside vertical electron density profiles. The basic selection criteria of these profiles are exactly the same that are explained in *Sánchez-Cano et al.* [2015a, 2015b]. Specifically for this study, these profiles come from areas without large crustal magnetic anomalies [*Acuña et al.*, 1999] because the objective is to understand the general behavior of the "normal condition" ionosphere across a long time period, and the presence of crustal magnetic fields can locally alter any ionospheric interaction with the solar wind. For similar reasons, data from orbits affected by strong and fast solar inputs, such as interplanetary coronal mass ejections (ICMEs) or co-rotating interaction regions (CIRs), were not considered because they need to be independently modeled. These data were identified primarily by using Earth as a monitor of the solar wind when Mars and Earth were in conjunction. Since this is not always the case, we looked at the magnitude of the magnetic field at the spacecraft altitude in the ionograms [see *Akalin et al.*, 2010]. The orbits were discarded when the magnetic field magnitude was larger than 50 nT and the field did not come from crustal fields as seen by the *Cain et al.* [2003] magnetic field model and also when a compressed Martian plasma system was observed due to the impact of these solar wind structures as described in, e.g., *Opgenoorth et al.* [2013].

Due to the Mars Express orbital evolution, there is an almost total absence of MARSIS AIS measurements for SZA smaller than 40° in periods C and D. As a consequence, and in order to avoid transport processes at the day-night terminator (SZA = 90°), this work is focused on data with SZA between 40 and 85°. Furthermore, when possible, AIS data were selected in order to cover the time interval of each solar cycle period as much as possible. However, for some specific time intervals (e.g., during MARSIS subsurface mode campaigns), the temporal coverage was limited by the scarcity of AIS data.

3. Ionospheric Behavior During Solar Cycle 23/24

3.1. Behavior of Topside Ionosphere in the Photochemical Region

The ionosphere can be described with the Chapman formulation if the basic assumptions described by *Chapman* [1931a, 1931b] are fulfilled, such as the atmospheric layers are horizontally stratified, electrically neutral, consist of a homogeneous gas formed by a single component with constant temperature, and remain in equilibrium. Additionally, the incoming radiation is monochromatic and each photon produces a single electron. The atmosphere has to be in hydrostatic equilibrium, and the neutral density of the atmosphere needs to decrease exponentially with altitude. Incoming solar radiation ionizes the neutral atmosphere. The solar flux is a maximum at the top of the atmosphere and decreases exponentially with altitude, as it interacts with the increasing neutral density. Due to a dynamic balance between the relative rates of ion production, loss processes, solar flux, and neutral population, an ionospheric layer is formed with at least one peak at an altitude which depends on this balance [*Rawer*, 1993]. The density profile, N (h), of this layer is defined as

$$N(h) = N_{\chi=0} \cdot \exp\left[\frac{1}{2}\left(1 - \frac{h - h_{\chi=0}}{H} - \mathrm{Ch} \cdot \exp\left(-\frac{h - h_{\chi=0}}{H}\right)\right)\right] \quad (1)$$

where $N_{\chi=0}$ and $h_{\chi=0}$ are the electron density and height of the maximum production rate when the Sun is overhead ($\chi = 0$) respectively, H is the neutral scale height, and Ch is the Chapman grazing incidence function [*Chapman*, 1931b], which includes the curvature of the atmosphere.

The shape of the vertical density profile is parametrized by the scale height, H. This parameter represents the vertical distance over which the density and pressure fall by a factor of 1/e. Physically, the scale height depends on the temperature (T) and composition (m) of the medium, as well as on the gravity (g) of the planet and the Boltzmann constant (K_B)

$$H = \frac{K_B T}{mg} \quad (2)$$

Table 1. Coefficients and Standard Deviation of the Modeled Scale Heights (Valid Between Solar Zenith Angles of 40 and 85°)[a]

(y = Slope·SZA + Intercept)		Period A	Period B	Period C	Period D
H_0 (km)	Slope	-0.00196	-0.01415	-0.09270	-0.04235
	Intercept	11.22	11.66	16.57	16.11
	SD	2.12	1.85	2.16	3.26
a	Slope	-0.00023	-0.00021	-0.00033	-0.00130
	Intercept	0.099	0.087	0.107	0.162
	SD	0.024	0.023	0.020	0.022

[a]SZA is in degrees, and SD is the standard deviation of H_0 and a, respectively.

This scale height can be used to define the behavior of both neutral and plasma (ions and electrons) components. However, this study has been done in relation to the neutral scale height since this is appropriate for the Chapman formulation as described above.

The Chapman formulation considers that the ionosphere in the photochemically controlled region can be represented with a constant scale height, H, as if it were uniform in composition and in temperature. Nevertheless, *Chapman* [1931a] predicted that H itself has a slow variation with height, which was, to a first order, neglected. Using AIS data from the MARSIS instrument, *Sánchez-Cano et al.* [2013] demonstrated that the Martian topside ionosphere is better reproduced with a neutral scale height with a linear variation in altitude, following the form

$$H = H_0 + a\,(h - h_0) \tag{3}$$

where H_0 is the neutral scale height at the peak layer, h_0 is the peak altitude, and a is the normalization factor which provides the degree of variation in altitude.

Each AIS topside profile suitable for this study was numerically fitted by a Chapman layer (equation (1)) with a linearly variable neutral scale height (equation (3)). The procedure is exactly the same as that followed by *Sánchez-Cano et al.* [2013]. At the end of the process, values for H_0 and a were acquired for each AIS profile. Then, linear regressions for the derived H_0 and a values as a function of the solar zenith angle were conducted for each solar cycle period. In principle, a is expected to have a linear variation with SZA and H_0 an exponential one [*Sánchez-Cano et al.*, 2013]. However in this work, we consider that a linear behavior for H_0 with respect to SZA better represents the data for the four solar cycle periods, as the linear fit and the exponential one described by *Sánchez-Cano et al.* [2013] give similar results. Finally, by using equation (3), an equation for the scale height, $H(h,\chi)$, is obtained for each solar cycle phase. The resulting fit coefficients, H_0 and a, from the linear fits and the standard deviation of the H_0 and a fits are shown in Table 1. As explained above, H_0 and a come from a linear fit whose slope and intercepted values in the ordinate axis are indicated in Table 1 for each phase of the solar cycle and SZA is in degrees. The final scale heights $H(h,\chi)$ for each solar cycle phase, which were obtained from the coefficients of Table 1, are plotted in Figure 2. H at the peak is in black, and the green line represents altitudes up to 50 km from the peak. Including the altitude range from the main peak up to 50 km above the main peak ensures that the analysis only covers the photochemical region. The results in Table 1 and Figure 2 show a statistically significant different behavior of the neutral scale height with the solar zenith angle for each phase of the solar cycle, which produce similar results to those of *Sánchez-Cano et al.* [2015b]. As expected, the lowest and largest values for all altitudes are found in the low and high solar activity phases, respectively (periods B and D). The only exception is period C for high SZA (SZA $>$ 70°) that has lower values of scale height than period B. For both moderate solar activity periods (A and C), a clearly different behavior is found with period C having a much larger dependence on the SZA. Moreover, the variation with SZA in periods A and B is relatively small, while periods C and D show a more pronounced dependence on this parameter.

Figure 3 shows the resultant topside Chapman profiles of ionospheric density (equation (1)) after considering the derived neutral scale heights (Table 1 and Figure 2). These profiles illustrate the behavior of the ionospheric density distribution for four different SZA values (in each panel) and for the different phases

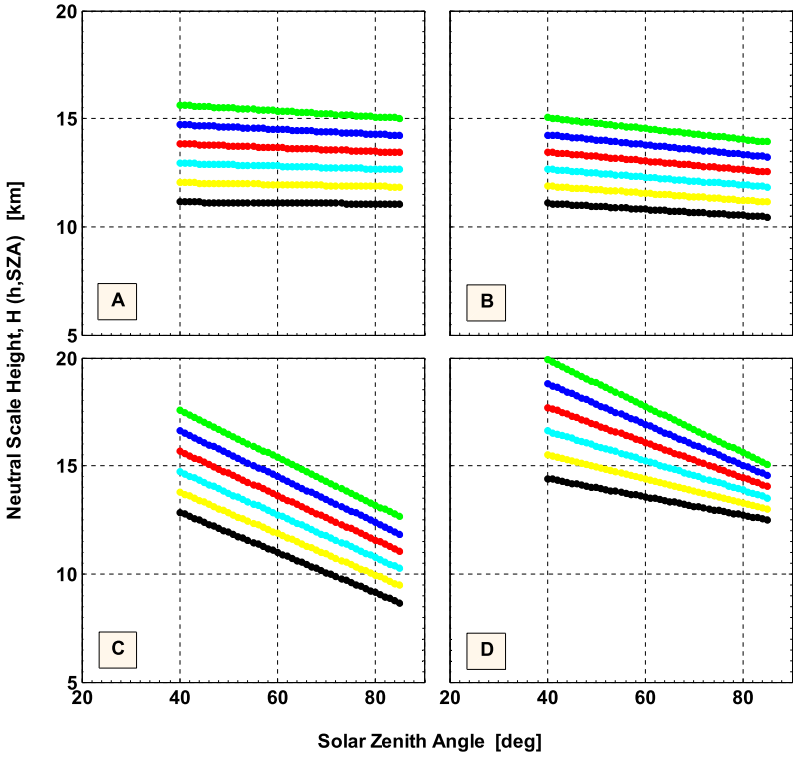

Figure 2. Neutral scale height variation obtained from MARSIS AIS data with altitude versus solar zenith angle for each of the four periods of solar activity. The coefficients of these curves can be found in Table 1. Each color corresponds to the following: black at the peak, yellow at 10 km, cyan at 20 km, red at 30 km, blue at 40 km, and green at 50 km above the main peak.

of the solar cycle (different line types and colors as described in the legend). The ionospheric profiles behave differently in response to each phase of the solar cycle and to SZA. Lower density values are found in the period of low solar activity (B, red solid profiles), indicating that during this period, the neutral temperature was colder than in the other three phases, as suggested by *Sánchez-Cano et al.* [2015b] and *Bougher et al.* [2015a]. The largest electron densities are found during the high solar activity level (period D, blue dashed-dotted profiles), as a result of the more intense solar radiation flux. The periods of moderate solar activity (A and C) represent transition phases between periods B and D. Generally, there is a relatively similar behavior with SZA during periods A and B, as the profiles from the declining phase are not far from the low solar phase profiles for all SZA, while periods C and D have a larger density variation with this angle.

3.2. Behavior of the Peak of the Main Layer

The evolution of the peak electron density behavior over a full solar cycle was recently analyzed by *Withers et al.* [2014]. They comprehensively sampled the peak electron density of the ionosphere of Mars over 15 years by combining radio occultation data from Mars Global Surveyor (MGS) and MARSIS AIS from Mars Express. The study focussed on the analysis of the peak electron density dependence on the solar activity, using the $F_{10.7}$ index, Lyman alpha emission and the Mg II core-to-wing index. They found that the peak density increases smoothly with these parameters, and even when the selection of observations was restricted to a narrow range of SZA and latitude, a time series of electron density residuals displayed notable trends, which may indicate a dependence of peak density on season, but not caused by changes in the Mars-Sun distance [*Withers et al.*, 2014].

Knowing that the different solar cycle phases create significant changes in the behavior of the topside electron density profile, and in order to complement the *Withers et al.* [2014] analysis, our study assesses the degree of deviation of the peak characteristics, both altitude and density, with respect to a reference

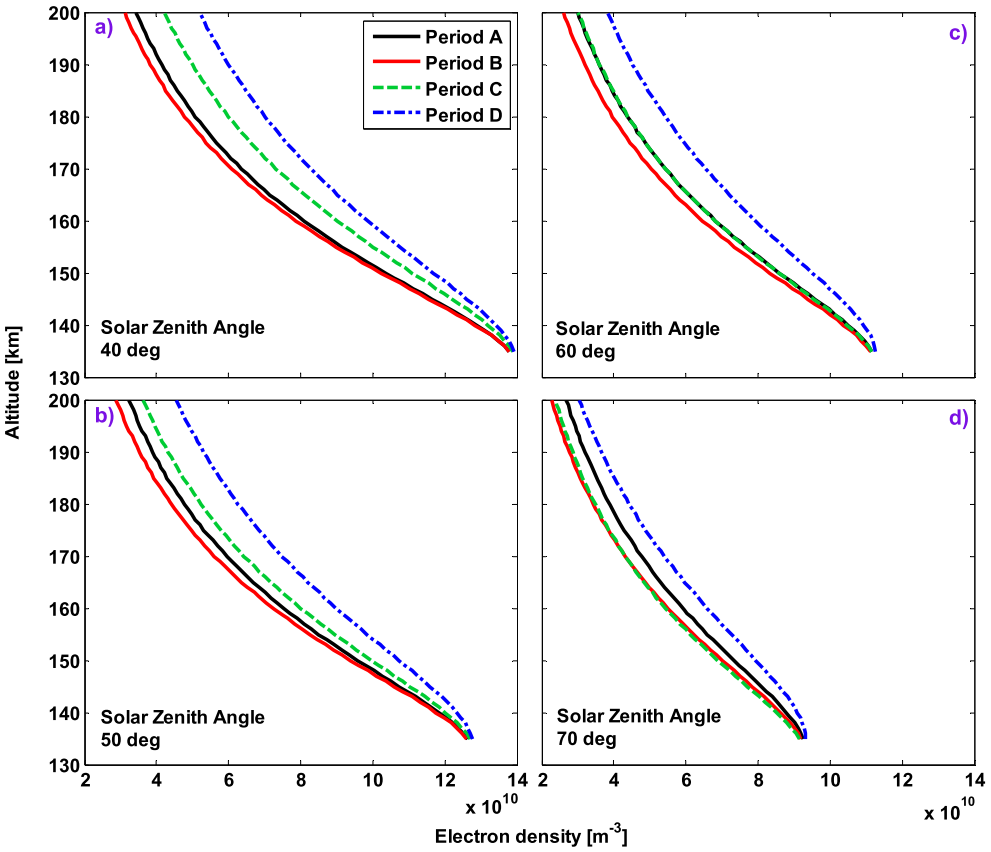

Figure 3. Modeled topside profiles from the new scale heights. Each panel corresponds to a different solar zenith angle and each line kind to a different phase of the solar cycle as marked in the legend.

ionosphere for each phase of the solar cycle. The empirical model of the ionosphere of Mars, called NeMars [*Sánchez-Cano et al.*, 2013], has been selected as a reference of the average ionospheric behavior. The model follows the Chapman formulation and calculates the electron density profile of the two main layers (photochemical region) of the ionosphere of Mars for nonmagnetized conditions (without data over regions with crustal magnetic anomalies and without data affected by solar wind induced magnetic field). The inputs of the model are the solar zenith angle, the solar activity (via the $F_{10.7}$ index), and the heliocentric distance. The main layer is based on the same data set as this study, AIS data, and the secondary layer is based on radio science data from MGS mission. In short, the modeled peak electron density of both layers depends on the SZA, $F_{10.7}$ index, and the heliocentric distance. On the other hand, the modeled peak altitude of both layers depends only on the SZA. The neutral scale height of the main layer varies with the solar zenith angle and the altitude from the peak and was obtained from Chapman fits to the observational AIS density profiles. The neutral scale height of the secondary layer is considered to be constant at 12 km. Therefore, although the model takes into account the solar activity for the peak density, it does not consider any variation with the different phases of the solar cycle. Therefore, an independent analysis of how the solar cycle affects the peak response can be made.

The aeroid altitude and the electron density of the main peak from the NeMars model have been directly compared with the peak observations of the AIS profiles. Regarding the electron density peak (Figure 4), the relative differences between the data and the model are close to zero for the solar cycle periods A, C, and D and can be considered inside the model uncertainty. The only exception is period B where a slight difference is found. Although the NeMars model considers the solar activity through the $F_{10.7}$ index as an input for the peak density calculation, the mean and median value of the distribution decreased by 7% with respect to the reference. The distribution shape is consistent with the other three periods but shifted to lower

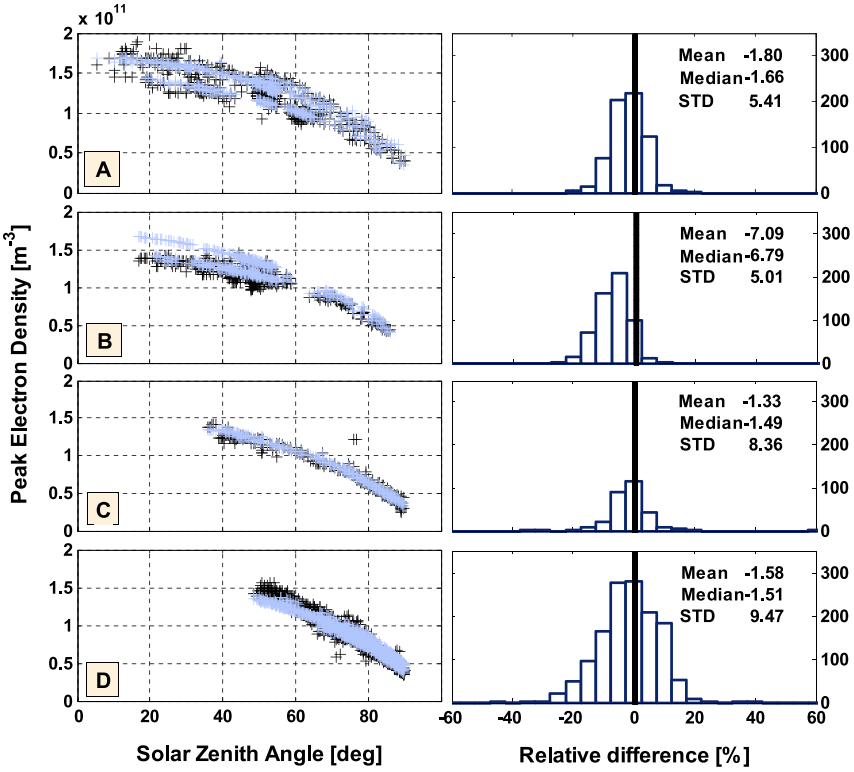

Figure 4. (left column) Peak electron density comparison between the real data obtained from the AIS profiles (in black) and the model outputs (in violet), for each phase of the solar cycle (in rows). (right column) Histograms of the relative differences between the real data and the model outputs for each phase of the solar cycle.

densities than estimated. The uncertainty in the local plasma frequency of the data is typically 3% or less [*Morgan et al.*, 2013], which is similar to the NeMars model [*Sánchez-Cano et al.*, 2013]. This is smaller than the above difference of 7% for the electron density peak in period B and is, therefore, statistically significant. This result suggests that the effect of the solar activity on the peak density may also be different, at least for the low activity solar cycle phase. We note a larger data spread during period D, as indicated by the standard deviation. Regarding the peak altitude (Figure 5), the statistical analysis indicates that for low and moderate solar activity phases (A, B, and C), the variations are very small: the mean and median of the relative differences are smaller than 2% (2.3 km in absolute difference) in all the cases, again inside the data error which is 6.9 km [*Morgan et al.*, 2013]. However, in the high solar activity phase (D), a larger variation in the peak altitude was found. In particular, the altitude decreased on average by about 8% (13 km in absolute difference) with respect to the model, this difference being more pronounced for high SZA. The distribution of period D also has the most spread shape as indicated by the histogram and standard deviation. Again, this variation is small but statistically significant. This difference suggests a different behavior during this solar cycle phase, especially for high solar zenith angles, because as seen in Figure 5d, the model predicts much higher altitudes than the current data for SZA $>$ 75°.

3.3. Behavior of Bottomside Ionosphere During the Latest Solar Minimum

The ionosphere below the main peak is strongly variable due to multiple factors, such as temperature changes, seasons, variations in the neutral atmosphere, dust storms, crustal magnetic fields, and solar flares [e.g., *Withers*, 2009, and reference therein]. In contrast to the vast amount of topside data that MARSIS has provided for the last decade, less information about the ionosphere below the main peak can be derived. From Mars Express, the observations of the ionospheric bottomside, or lower ionosphere, during the latest solar cycle come from the Mars Radio Science (MaRS) experiment [*Pätzold et al.*, 2009; *Peter et al.*, 2014], which provides complete electron density profiles from the ionopause down to the base of the ionosphere. The MaRS data set coverage is significantly smaller than the MARSIS data set because

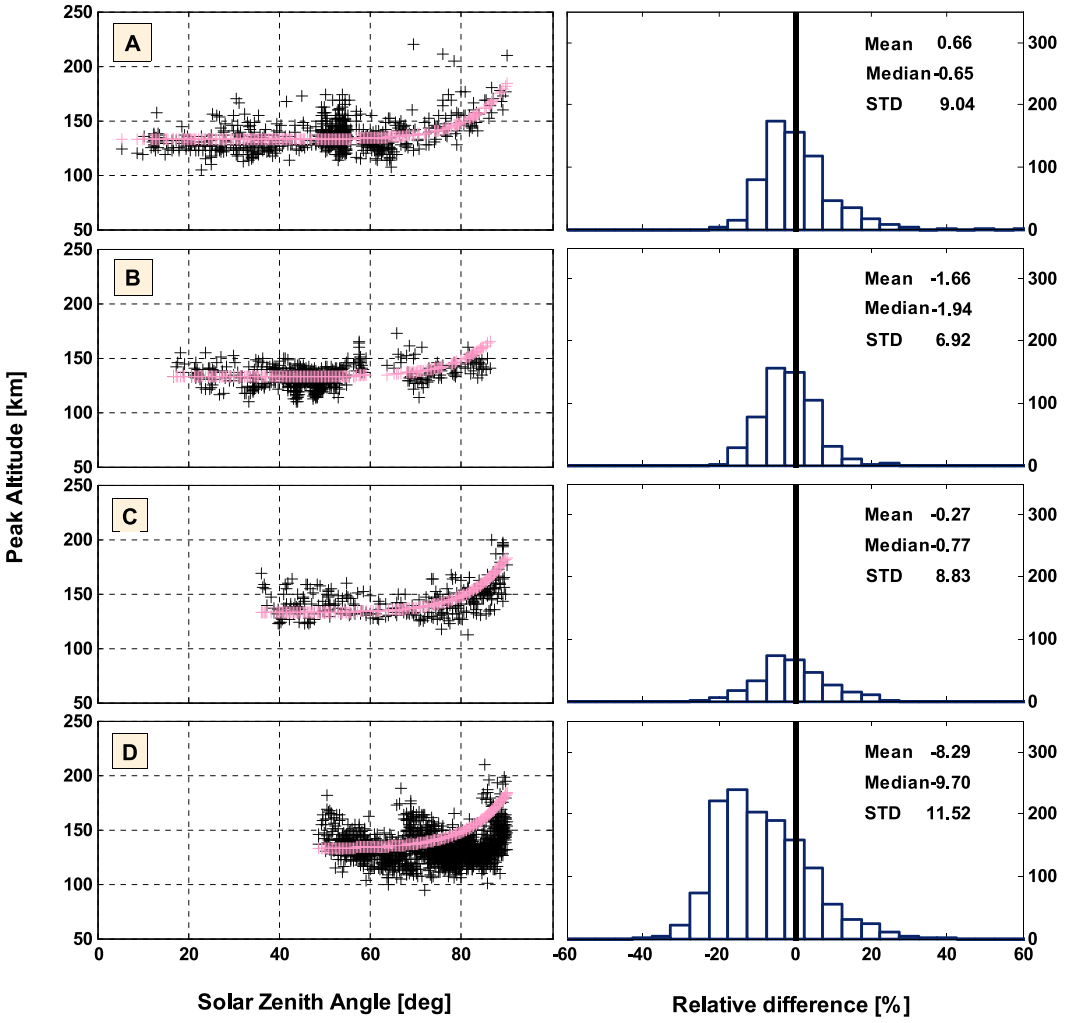

Figure 5. Same as Figure 4 but for the peak altitude.

the instrument requires an occultation (the spacecraft is occulted by Mars from the Earth's point of view), which only occurs during limited time periods (called occultation seasons) and only once per orbit [*Pätzold et al.*, 2009]. Due to these geometrical constraints, data are recorded during occultation seasons only in the SZA range from 48 to 132°.

The MaRS data set can be used to trace the general behavior of the lower ionosphere, especially the secondary layer, during the long solar minimum. As seen in Figure 1, the period of extreme low solar activity was characterized by an almost absolute lack of measurable solar X-rays. Short wavelength solar photons penetrate deepest into the atmosphere of Mars and, due to their high energies, create a large amount of secondary electrons in the altitude region around the secondary layer [*Peter et al.*, 2014]. A detailed analysis of the behavior of secondary electrons can be found in *Nicholson et al.* [2009]. Due to the reduction of solar X-rays, a strong decrease in the ionization below the main peak is expected. To check this hypothesis, 12 radio science profiles were selected, where all profiles were observed for SZA between 71 and 82°, and in surface areas without crustal magnetic field influence, to cover the four solar activity periods (Figure 6 and Table 2). Despite the high SZA conditions and the large variability always present in the lower ionosphere, the general trend observed in Figure 6 agrees with the proposed hypothesis. Electron density profiles from period B show a behavior different from that found in all other solar activity periods. The secondary layer is nearly absent, most possibly due to the absence of solar X-ray radiation, while in the other three periods, this layer is obvious. Moreover, the fast decay of density from the main

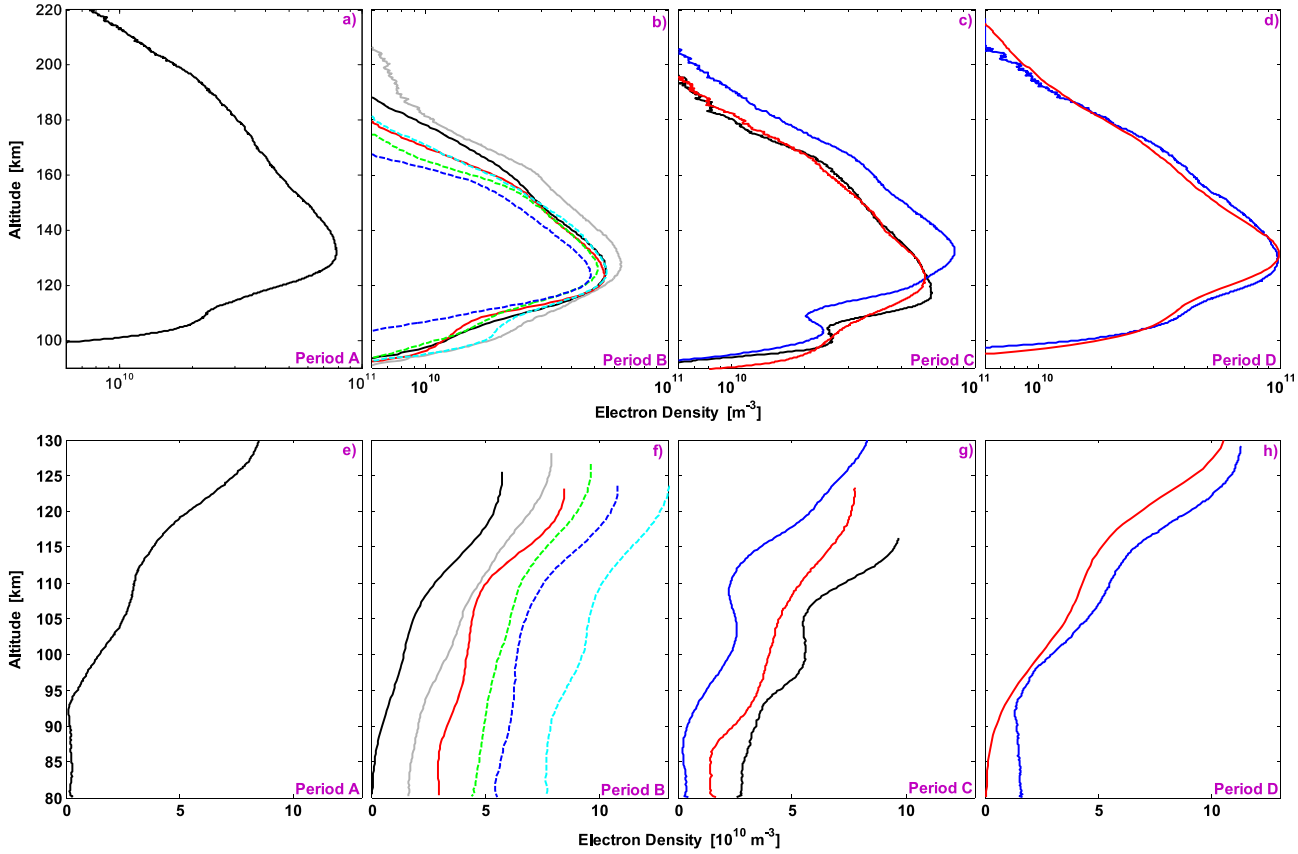

Figure 6. MaRS profiles of the four solar cycle periods. (a–d) The full profiles in the same scale. (e–h) A zoom in of the bottomside of the profiles in Figures 6a–6d, with same color to help in the identification. Profiles in Figures 6e–6h have been shifted by $1.5 \cdot 10^{10}$ m^{-3} in density in order to help to visualize every profile separately. All the profiles belong to areas without crustal magnetic field. Solid line profiles are from solar zenith angles between 71 and 79°. Dashed line profiles are from solar zenith angles between 80 and 82°. See Table 2 for more information.

peak to lower altitudes shown by these profiles from period B is similar to the fast decay of the electron density of the terrestrial *E* layer [*Rees*, 1989].

In addition to the findings for the secondary layer, the selected MaRS data subset is consistent with the observations of the ionospheric topside in the previous sections. The MaRS profiles from period B show a clearly reduced topside density in the same manner as the MARSIS AIS data set for that period (section 3.2).

Table 2. Orbital Characteristics of the MaRS Radio Occultation Profiles in Figure 6

Solar Cycle Period	Earth Date	Mars Express Orbit Number	SZA (deg)	d_{M-S} (AU)	*Ls* (deg)	LTST (h)	$F_{10.7}$ (Solar Flux Unit, sfu) at 1 AU	X-ray Background Flux (W/m^2) at 1 AU
A	1 May 2007	4262	71.64	1.39	229	10.78	86	$3.8 \cdot 10^{-8}$
B	27 Jul 2008	5865	82.44	1.64	104	13.15	66	Less than $0.0 \cdot 10^{-8}$
B	27 Jul 2008	5866	82.36	1.64	104	13.17	66	Less than $0.0 \cdot 10^{-8}$
B	3 Aug 2008	5890	80.36	1.63	107	13.63	66	Less than $0.0 \cdot 10^{-8}$
B	7 Aug 2008	5904	79.43	1.63	109	13.86	66	Less than $0.0 \cdot 10^{-8}$
B	8 Aug 2008	5908	79.16	1.63	109	13.93	66	Less than $0.0 \cdot 10^{-8}$
B	8 Sep 2008	6016	76.29	1.60	124	15.45	67	Less than $0.0 \cdot 10^{-8}$
C	10 Oct 2009	7404	71.71	1.54	352	12.60	70	Less than $0.0 \cdot 10^{-8}$
C	17 Jun 2010	8267	78.29	1.64	105	12.96	70	$4.2 \cdot 10^{-8}$
C	19 Jun 2010	8274	77.98	1.63	106	12.97	69	$4.2 \cdot 10^{-8}$
D	23 Jun 2011	9539	71.20	1.45	315	06.62	96	$1.7 \cdot 10^{-7}$
D	25 Jun 2011	9547	71.91	1.45	317	06.53	94	$1.7 \cdot 10^{-7}$

Furthermore, the density is the largest during high solar activity as expected from the previous analysis. The same is observed with respect to the peak density, where a clear reduction is found in the profiles of period B in relation to the other three solar cycle phases.

While Figures 6 and 10 of *Peter et al.* [2014] show that the TEC value is dominated by the amount of available ionization in the main peak, a strong reduction of the topside and lower ionosphere, as found in period B, may produce anomalously low TEC values. This topic is discussed in the next subsection.

3.4. Total Electron Content

The TEC is an estimate of the number of free electrons along the path crossed by the radar signal. Therefore, it is used to monitor the amount of ionization of the ionosphere, as well as its variability in time and space. Using the MARSIS instrument, TEC can be derived independently from both operational modes: the AIS mode provides TEC estimates only for the topside of the ionosphere by doing the integration with altitude of the electron density, while the subsurface sounding mode provides TEC for the entire ionosphere derived as a by-product from the analysis of signal distortion caused by the dispersive ionosphere [*Sánchez-Cano et al.*, 2015a]. In principle, TEC for the entire ionosphere can be estimated measuring the time delay of the surface echo in the AIS mode, but the accuracy of this determination appears to be low [*Gurnett et al.*, 2008]. In this subsection, we make a comparison and evaluate the differences between the full atmosphere TEC data set from MARSIS subsurface mode and the TEC data set obtained from the MARSIS AIS scale heights of section 3.1 with the help of the NeMars model. The two estimates of TEC are entirely independent.

To analyze the evolution of the TEC within the entire ionosphere across the solar cycle, subsurface TEC estimates from the *Cartacci et al.* [2013] algorithm have been exploited. Figure 7 shows the daily evolution of the Martian ionospheric TEC (in blue) in the interval from the deployment of MARSIS (July 2005) to mid-2012. These data correspond to the daily average TEC evaluated during the dayside, i.e., SZA between 60 and 79°. Data only close to the terminator region have been selected as the most accurate as are assessed by *Sánchez-Cano et al.* [2015a]. A threshold has been applied to the signal-to-noise ratio (SNR) such that only data with a SNR $\geq$ 25 dB are used. This conservative approach is due to the fact that for a lower SNR, the accuracy of the TEC estimation could be affected by signal degradation. Note that when the radar works in the subsurface mode, it cannot take measurements throughout the full dayside because the carrier frequencies are smaller (or of the same order of magnitude) than the plasma frequency, and therefore, the radar signals do not penetrate properly into the ionosphere [*Sánchez-Cano et al.*, 2015a]. This leads to strong signal phase distortion and consequently substantial losses in terms of SNR. As observed in Figure 7, the daily TEC is strongly influenced by the heliocentric distance of Mars, illustrated by the sinusoidal shape of the curve and the general trend which evidently follows the EUV solar radiation pattern (Figure 1c), as expected. Moreover, the solar cycle phases also play an important role in the global TEC, which is clearly reduced during period B and increased during period D, both with respect to the moderate solar cycle phases.

The NeMars model was run for the daily conditions of all observations used for Figure 7 in order to make a comparison and evaluate the differences obtained with respect to the full atmosphere TEC obtained from MARSIS subsurface data set. Since the neutral scale height of NeMars does not take into account any solar cycle phase considerations, apart from the variation in $F_{10.7}$ of the peak density, the four new neutral scale heights obtained in this study (see section 3.1) have replaced the original one in the corresponding time periods. Moreover, according to section 3.2, a peak density reduction of 7% and a peak height reduction of 8% were included for periods B and D, respectively. Regarding the bottomside (or lower ionosphere), for both moderate and high solar activity phases, it was decided to run the NeMars model without any modification. For the case of the low solar activity phase (period B), however, there is some evidence of a significant reduction of the bottomside main ionospheric layer in the MaRS data subset. Consequently, the NeMars model has been run with the new scale height for this solar phase and with only the main layer in this period. Figure 7 shows the modeled TEC (red line), which was obtained from a numerical integration of the model electron density distribution in altitude. The black lines correspond to the calculated TEC from the scale height with added standard deviation shown in Table 1. Note that the steps between periods in the modeled TEC are an artifact of dividing the interval into four subintervals. Taking into account that the uncertainty of the plasma frequency and altitude of the AIS data set is typically 3% or less and 6.9 km, respectively, and that the sensitivity of the derived TEC from subsurface mode is about $3.8 \cdot 10^{14}\,\mathrm{m}^{-2}$ in the dayside [*Sánchez-Cano et al.*, 2015a, and references there], the agreement between them is good. This comparison demonstrates

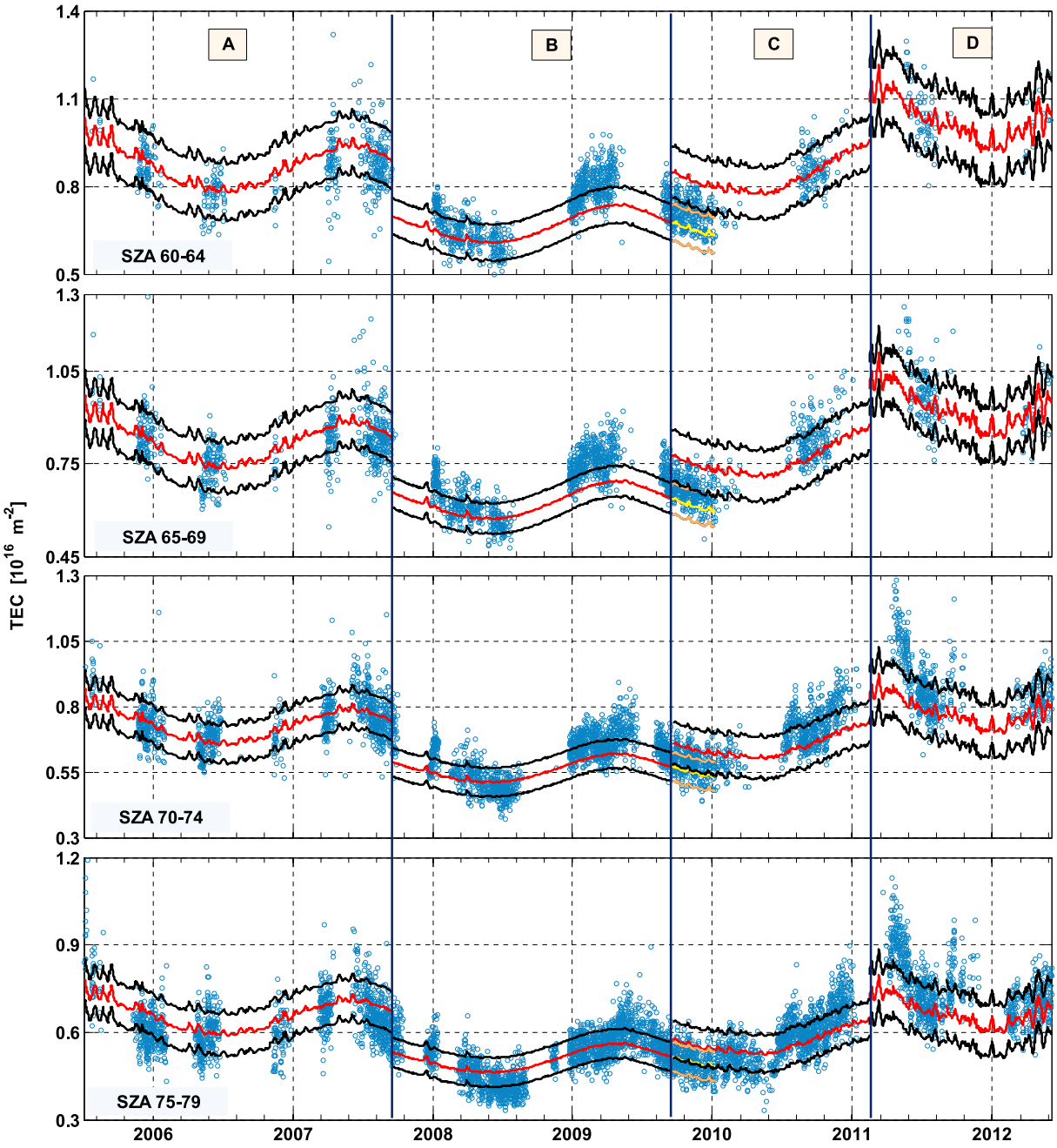

Figure 7. TEC of the full ionosphere measured by MARSIS in the subsurface mode (blue) over the full solar cycle covered by MARSIS instrument. TEC corresponds to the daily average value evaluated during the dayside, i.e., solar zenith angles between 60 and 79°, and only considering data with a SNR $\geq$ 25 dB. In this figure, subsurface data set starts on 4 July 2005 and finishes mid-2012. Additionally, the modeled TEC of the two main layers in the ionosphere has been plotted (red line), after considering in each period the new neutral scale heights. As described in the text, note that only the main layer has been considered during the period of low solar activity. The model was run for the mean solar zenith angle in each period showed in the figure. The black lines stand for the TEC calculated from the scale height standard deviation shown in Table 1. The yellow and salmon lines of period C correspond to an extrapolation of the model curves of period B.

that the empirically modeled scale height of each period from the AIS data (section 3.1) is consistent with independent empirical observations, i.e., subsurface-derived TEC.

Some specific differences are, however, noticeable. The agreement in period A (moderate solar activity, declining phase) is the best of the four periods for all four solar zenith angle ranges. In period B (low solar activity phase), the agreement is very good especially from the end of 2007 to the start of 2008, for

SZA $< 75°$. This is a clear indication that the ionization under the main peak disappeared in a permanent form during that time due to a lack of X-ray radiation produced at the Sun since the secondary layer is not included in the model. For SZA $> 75°$, although the agreement is not bad, the subsurface TEC is smaller than the model, which can be explained by a larger bottomside reduction (including the main layer bottomside), which by design the model does not consider, or a larger reduction in the scale height of the main layer which was not indicated by data from the MARSIS AIS mode. However, the largest differences are observed during 2009 for lower SZAs ($<75°$). In this case, the model provides lower values by up to about $0.2 \cdot 10^{16}$ m^{-2} than the data retrieved from the subsurface sounder.

In period C (moderate solar activity, ascending phase), for solar zenith angles higher than 70°, both data sets agree well. For lower solar zenith angles, however, a notable discrepancy is found from the beginning until mid-2010. It seems that the full ionospheric TEC followed a similar trend to that during the low solar activity period, with the yellow and salmon colored lines which correspond to an extrapolation of the model of period B. This suggests either a smaller scale height, not obtained from the AIS profiles in this period, or a lower ionization in the bottomside. However, in principle, a "normal" behavior for the bottomside is expected since the X-rays and EUV solar flux were clearly increased with respect to period B, the lowest levels (see Figure 1). It is likely that this is more a result of dividing the interval into four subperiods. The real transition between periods will have been more gradual than the modeled one, which by design cannot predict the transition period behavior.

Finally, in period D (high solar activity phase), although there is not a large number of available data, the agreement is reasonable. The more pronounced differences appear again just at the start of the period, where the largest subsurface TEC of the whole interval is observed but not reproduced by the model. This could be a consequence of the Mars Express trajectory, as these data were recorded mostly during April 2011, when the spacecraft was traveling over the Southern Hemisphere and lower latitudes of the Northern Hemisphere. The high values of the TEC estimates could be related to the interaction of the ionosphere with the local magnetic field, mainly localized in the Southern Hemisphere. As *Cartacci et al.* [2013] demonstrated, regions of enhanced TEC preferentially correspond to areas of high magnetic field intensities where the field lines are quasi-perpendicular to the Martian surface. In the particular case of SZA between 70 and 79, the TEC and SNR were high, while for higher values of SZA, the distortion increases and the SNR drops rapidly. On the contrary, the AIS-derived neutral scale heights were calculated from AIS data away from these magnetized regions.

4. Ionospheric Temperature Evolution With Solar Cycle

The average temperature of the medium for a given altitude is a useful by-product of the scale height and is easily derived from equation (2). Taking advantage of the four neutral scale heights obtained in this study (Table 1), the typical neutral temperature during the solar cycle has been calculated. This definition is only valid for a medium in hydrostatic equilibrium, with a constant temperature, and supposing that the observed electron density mirrors the neutral temperature and is not influenced by the ion or the electron temperatures. In the case of Mars, this is only valid in the so-called photochemical region, i.e., altitudes below 170–200 km. Therefore, in order to avoid nonphysical results, the neutral temperature was derived from the neutral scale height only at the altitude of peak ionospheric densities, typically 130 km. To do this, the mass of CO_2 (main neutral component) and Mars's gravity at the peak altitude were used.

Moreover, primary information of the temperature of the plasma components (ions and electrons) can also be retrieved for the very closest region to the peak. This temperature can affect both the chemistry and dynamics of the plasma and is a key factor for ionospheric modeling. For example, for higher plasma temperatures, the photochemical recombination rate decreases, and therefore, the plasma scale height increases because the ion production rate dominates over the ion loss rate. The plasma scale height, *Hp*, can be calculated from equation (4), which basically gives the slope of the electron density profile in altitude

$$Hp = -\frac{\mathrm{d}h}{\mathrm{d}(\ln N)} \tag{4}$$

where h is the altitude and N is the electron density. The procedure for obtaining *Hp* along the solar cycle was as follows: the main layer profile was reconstructed by using the empirical model NeMars, based on the Chapman formulation, and previously described. To run the model, the NeMars neutral scale height was replaced by the four new empirical neutral scale heights calculated in section 3.1 for each period of the solar

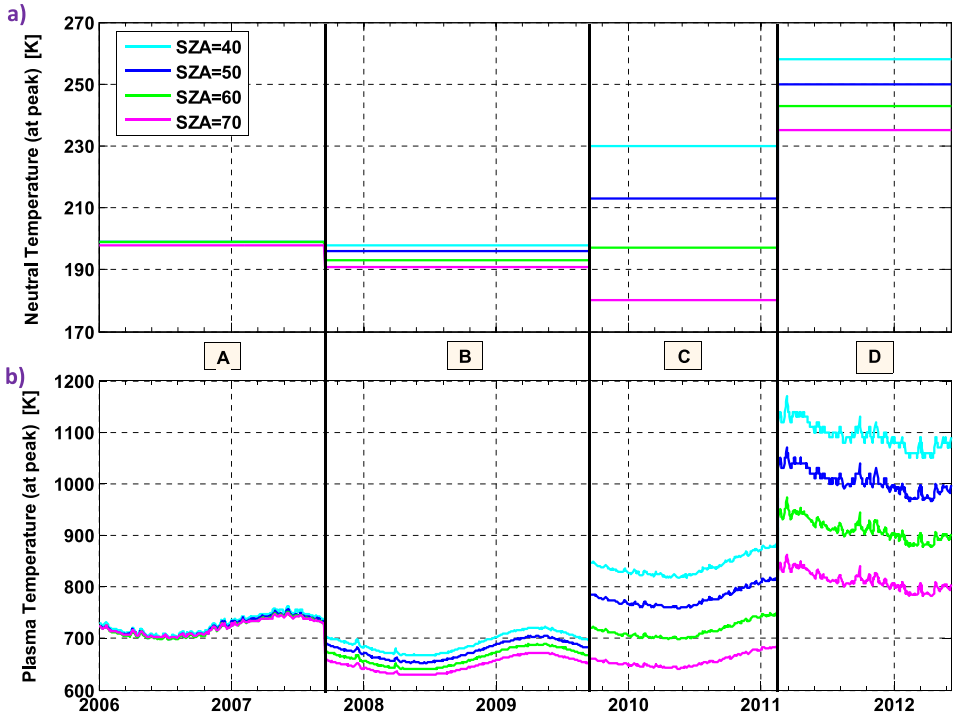

Figure 8. Evolution of the average (a) neutral and (b) plasma, electron, and ion temperatures at the peak ionospheric region derived from both the neutral and plasma scale heights, respectively, with solar cycle. In both cases, four different solar zenith angles have been plotted as indicated in the legend.

cycle. For periods B and D, according to section 3.2, a peak density reduction of 7% and a peak height reduction of 8% were included, respectively. Then, the best linear fit of the closest region to the peak of the modeled profiles (in logarithm scale) was made for the altitude region between the peak and the height where the electron density was reduced by 25%. The 25% density reduction is reached, generally, between 20 and 30 km above the peak (within the photochemical region). From these best fits, the slope provides the plasma scale height as described in equation (4). Finally, the plasma temperature (electrons and ions) can be derived from equations (2) and (4), after considering that O_2^+ is the major ion at the main peak altitude, as Mars Atmosphere and Volatile EvolutioN (MAVEN) mission has recently confirmed [*Bougher et al.*, 2015b].

Figure 8 shows the evolution of the average neutral and plasma temperatures at the peak region derived from both scale heights during the solar cycle. In both cases, four different SZAs have been considered. Note that as in the TEC case, the steps between periods are due to the divisions applied in the solar cycle to model the neutral scale height. Regarding the neutral temperature, a constant value for the peak altitude is obtained in each solar cycle phase because this parameter comes directly from each of the four scale heights obtained in section 3.1. Therefore, this temperature should be treated as the average temperature of each solar phase. Nevertheless, a variation with the Sun-Mars distance is expected, similar to the one showed in the *Bougher et al.* [2015a] solar activity/season temperature maps. On the other hand, the plasma temperature (ions and electrons) is a useful by-product obtained from an observations-model combination. Consequently, Figure 8b shows that the plasma temperature has a variation with solar activity and heliocentric distance, because the peak electron density in the NeMars model depends on them.

Globally, both temperature variations are similar to the solar cycle variation (Figure 1). This is a notable result since this plot was obtained from the independent analysis of the scale height, which means directly from AIS data, and not from the solar radiation flux data (Figure 1 was used to split the data, but not used as input). It is clear that both temperatures have the highest and lowest values at the high and low solar activity phases, respectively. This fact corroborates the findings of *Sánchez-Cano et al.* [2015b], which indicate that Earth and Mars have a similar response to changes in the solar cycle. The only exception is period C for high SZAs where a very close variation to the period B is found in the plasma population, as well as a further

cooling of the neutral component. This cooling of 10 K in period C is directly related to the neutral scale height observations (Figure 2), where close to the terminator (SZA $>$ 75°) the neutral scale height at the peak (black lines in Figure 2) is smaller than in other periods. Therefore, as T and H are directly proportional (equation (2)), the lower the scale height, the smaller the temperature. Finally, we highlight a significant temperature variation with SZA only for the ascending and high phases of the solar cycle (periods C and D). Recall that the temperature behavior comes from the scale height, and, therefore, it is similar to the behavior of the scale height shown in Figure 2 (black lines). The difference, on average, reaches 50 K for SZA between 40 and 70°.

More specifically, the temperatures shown in Figure 8 are consistent with previous observations. The neutral temperatures obtained for the period A corroborate observations from Ultraviolet and Infrared Atmospheric Spectrometer (SPICAM) Mars Express data in the first years of the Mars Express mission [*Leblanc et al.*, 2006], where the average temperature deduced from dayglow emission scale heights between 150 and 190 km was 201 ± 10 K, without any significant variation with respect to the SZA. Figure 10 of *Leblanc et al.* [2006] indicates that the neutral temperatures derived from the SPICAM data are almost the same as those obtained in this work. Similarly, our results are comparable to those shown in *Forget et al.* [2009] at 130 km. Regarding the low phase of the solar cycle (period B), our findings are consistent with those obtained from missions in previous solar minima. From the aerobraking phase of MGS, a temperature of 200 K was derived above 150 km for the dayside [*Keating et al.*, 1998], not far from the 185–200 K derived from the Vikings' measurements [*Hanson et al.*, 1977]. In the ascending phase of solar cycle (period C), the results are similar to those based on MGS orbital period changes where the temperatures varied between 180 and 320 K for the period 1999–2005 [*Forbes et al.*, 2008]. Finally, for the high solar cycle phase (period D), *Stewart* [1972], using dayglow emission scale height data from Mariner 6 and Mariner 7, indicated that the observed CO Cameron band emission scale height of 19 km suggested an exospheric temperature of 315 ± 75 K. And modeling of the ionosphere composition based on the observations results in a variation between 278 and 390 K at 135 km of altitude. Therefore, our results, although a bit lower, are in the range of those obtained by *Stewart* [1972]. A complete summary of all the available neutral temperature data can be found in *Stiepen et al.* [2015]. Regarding neutral temperature values obtained by modeling, *Bougher et al.* [2015a] using the Mars global ionosphere-thermosphere model (MGITM) recently simulated the solar cycle variations of the Mars upper atmosphere. They predicted a solar cycle variation of the maximum temperature in the dayside between 215 and 350 K at 200 km of altitude. Taking into account that our study focused at the peak altitude (on average 135 km), the results are consistent with the *Bougher et al.* [2015a] findings, although we find for high solar activity a more moderate neutral temperature.

Regarding the plasma temperature, our results of low solar activity phase are in good agreement with the two single ion temperature profiles measured by the descending module of both Viking spacecraft [*Hanson et al.*, 1977; *Hanson and Mantas*, 1988], as can be extrapolated from Figure 10 in *Hanson et al.* [1977] and Figure 4 in *Hanson and Mantas* [1988]. For high solar activity phase, our results can be compared to the recent MAVEN measurements of electron temperature. *Ergun et al.* [2015] show that for 15° of solar zenith angle, the electron temperature is ~0.052 eV at 130 km (~600 K). We expect that our results are lower than this quantity, as we are only analyzing SZA $>$ 40°. Taking this into account, our results are in agreement to those of MAVEN shown in *Ergun et al.* [2015], if for the peak region the ion temperature is approximately equal to the electron temperature as the Viking landers recorded [*Hanson et al.*, 1977; *Hanson and Mantas*, 1988]. An indirect comparison can also be done from the radio occultation profiles acquired by Mars Global Surveyor mission. In a recent paper, *Cui et al.* [2015] derived the electron temperature at the peak of the electron production, which varied between 320 K and 570 K between 1998 and 2005. The study presented in this paper focuses on the electron plus ion temperatures, which are consistent with the *Cui et al.* [2015] results if, as before, both electron and ion temperatures are considered approximately equal at the peak region.

5. Pressure Balance and Induced Magnetic Field During the Latest Solar Cycle

The solar wind interaction with nonmagnetic planets/bodies, like Venus, Mars, or Titan, has been largely postulated and empirically confirmed by missions [e.g., *Russell and Vaisberg*, 1983; *Shinagawa and Cravens*, 1989, 1992; *Zhang and Luhmann*, 1992; *Bertucci et al.*, 2005; *Dubinin et al.*, 2008; *Edberg et al.*, 2008, 2009; *Akalin et al.*, 2010; *Bertucci et al.*, 2015]. In general, when the solar wind finds a nonmagnetized obstacle, a bow shock is formed in the flow and the solar wind plasma continues to slow down (in the magnetosheath) as it

approaches the ionopause [*Cravens*, 1997]. The flow stagnates just upstream of the subsolar ionopause, and the dynamic pressure is converted into thermal pressure, as described by the following set of equations:

$$P_{sw} + P_B = P_{th} \tag{5}$$

$$P_{sw} = 0.85\, \rho_{sw}\, u_{sw}^2\, \cos^2\chi \tag{6}$$

$$P_B = \frac{B^2}{2\mu_0} \tag{7}$$

$$P_{th} = N_e\, K_B (T_e + T_i) \tag{8}$$

where P_{sw} represents the solar wind dynamic pressure, P_B the magnetic field pressure due to the solar wind, and P_{th} the thermal pressure of the ionosphere. In addition, the constant, 0.85, in equation (6) depends on the ratio of specific heat for the hypersonic solar wind flow; ρ is the solar wind density calculated as $\rho_{sw} = 1.18 \cdot n \cdot m$, where n and m are proton density and mass, respectively. The factor 1.18 accounts for the helium abundance in the solar wind, which is about 4.5% [*Zhang and Luhmann*, 1992, and references there]; u is the speed of the solar wind, χ is the solar zenith angle, B is the magnetic field magnitude due to the solar wind, μ_0 is the magnetic permeability in the vacuum, N_e is the ionospheric electron density, K_B is the Boltzmann constant, and T_e and T_i are the electron and ion temperature, respectively.

As the flow slows down, magnetic field lines "pileup" outside the ionopause. Theoretically, as described in *Cravens* [1997] (or in any other general basic reference), the ionosphere from the point of view of the balance of pressures can exist in two states: (1) unmagnetized or (2) magnetized. The first state (unmagnetized ionosphere) seems to occur whenever the solar wind dynamic pressure is substantially less than the maximum ionospheric thermal pressure (thermal pressure at the peak of the ionosphere). This is the most common state of the ionosphere of Mars. Here the ionopause can be treated as a tangential discontinuity at which the magnetic pressure on the magnetic barrier side balances the ionospheric thermal pressure ($P_B = P_{th}$). In this situation, B is the strength of magnetic field at the bottom of the magnetic barrier. In the case of Venus, it was empirically demonstrated that the peak magnetic pressure in the magnetic barrier is approximately equal to the solar wind dynamic pressure upstream of the bow shock [*Russell and Vaisberg*, 1983]. The second state (magnetized ionosphere) seems to occur when the solar wind dynamic pressure is comparable to or greater than the maximum ionospheric pressure (at the peak of the ionosphere). In this case, an induced magnetic field is expected at ionospheric altitudes because the thermal pressure is no longer sufficient to balance the solar wind pressure. Therefore, the ionopause should be found closer to the planet and in a wider altitude interval than in the unmagnetized state.

The objective of this section is to investigate in which parts of the solar cycle the ionosphere were weaker in relation to the solar wind dynamic pressure and, therefore, the possibility of being in a magnetized state more easily in comparison to other periods.

Some previous evidence was found for the period of low solar activity by *Sánchez-Cano et al.* [2015b]. They showed with a case study that the differences in both electron density and neutral scale height observed during the period of extreme low solar activity in 2008 and 2009 were most probably due to the presence of an induced magnetic field at lower ionospheric altitudes than in the other phases of the solar cycle. The probability of existence of any of these two ionospheric states during the last solar cycle is here analyzed by comparing the solar wind dynamic pressure and the maximum thermal pressure over the time, since, as theoretically described above, the topside ionosphere shape depends on the balance between them. Therefore, if the relationship between these two parameters is smaller, the ionosphere will be more compressed and the topside scale height will be reduced.

Figure 9a shows the solar wind pressure at Mars's location during the last solar cycle. This parameter was calculated for different SZAs by using equation (6). Data come from the ACE satellite (up to 23 August 2011 because a radiation and age-induced hardware anomaly altered the instrument's operational state of the ACE satellite) and from OMNI (Operating Missions as a Node on the Internet) (from 23 August 2011 to the end), both at 1 AU. To extrapolate them to Mars, the proton density (n) was normalized by the square of the Mars-Sun distance, and the solar wind speed (u) was considered to not vary substantially with radius [*Zhang and Luhmann*, 1992] and is assumed to be that at 1 AU. We note that this is the first approximation to the real value of the solar wind pressure at Mars because it is not necessary that the solar wind pressure behavior has to be similar at the two planets when they are not aligned. Nevertheless, since there are no

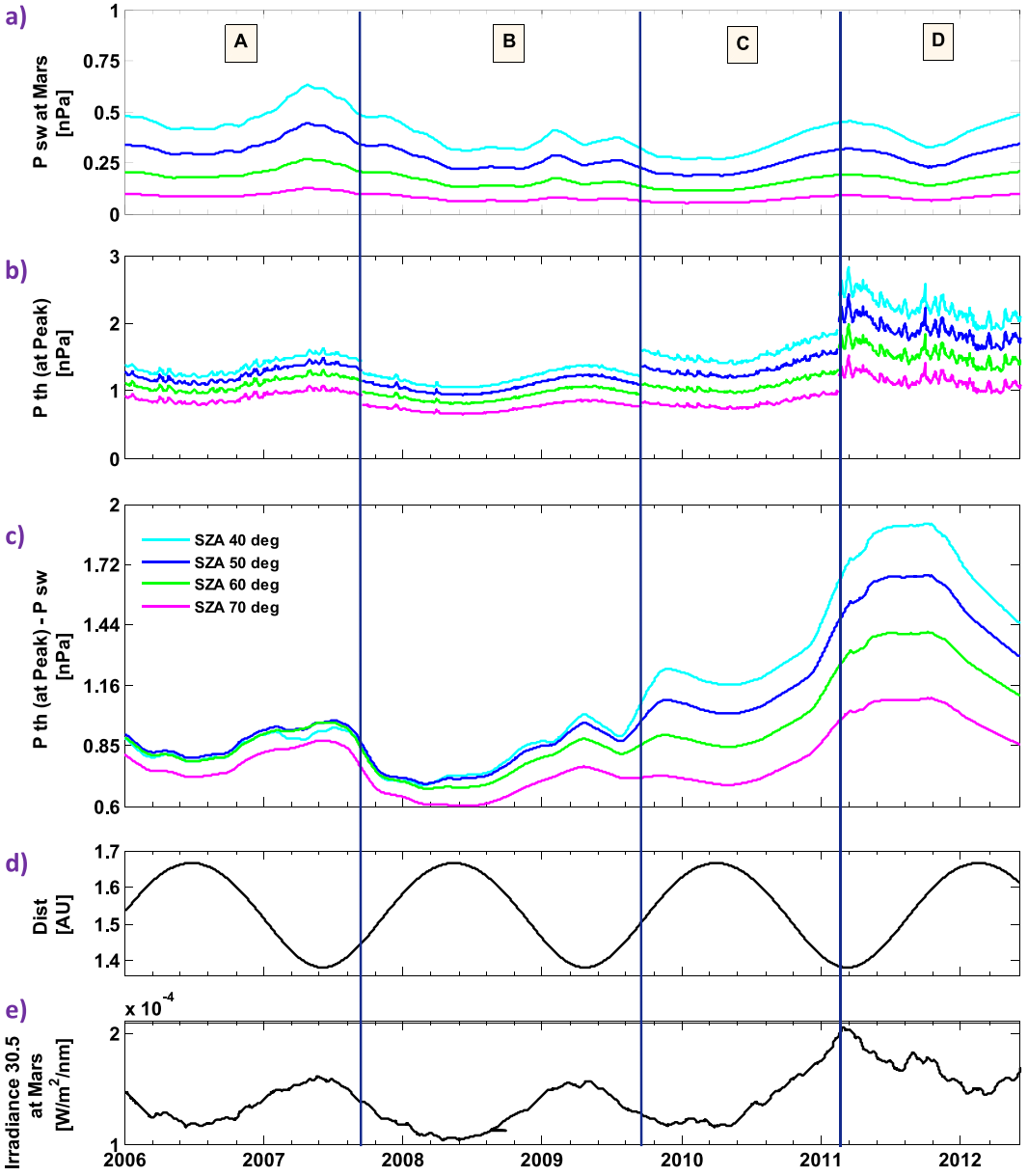

Figure 9. (a) Evolution of the solar wind pressure at Mars's location, calculated for different solar zenith angles with data at 1 AU after normalization to the Mars position. (b) Evolution of the peak thermal pressure (maximum thermal pressure at the main peak of the ionosphere), calculated for different solar zenith angles from the plasma scale height at the main peak of the ionosphere. (c) Evolution of the pressure difference between the maximum thermal pressure and the solar wind pressure. Note that the vertical scale is not the same in Figures 9a–9c. (d) Mars heliocentric distance. (e) EUV solar irradiance at 30.5 nm scaled to Mars distance.

accurate measurements of the solar wind pressure at Mars for the entire solar cycle (daily) yet (work currently in progress by Analyzer of Space Plasmas and Energetic Atoms Mars Express team (ASPERA-3)), this is the only approach that can be done for this interval. In Figure 9b, the peak thermal pressure (maximum $P_{th,}$ at the peak of the ionosphere) during the last solar cycle is shown. This parameter was calculated for different SZAs by using equation (8), where $(T_e + T_i)$ comes from the plasma scale height (equations (2) and (4)). For periods B and D, according to section 3.2, a peak density reduction of 7% and a peak height reduction of 8% were considered, respectively. These two kinds of empirically derived pressures are in full agreement with previous results [see, e.g., *Zhang and Luhmann*, 1992]. Therefore, as described above, from the difference between these two pressures, the relationship between them can be obtained, and thus, in which periods, a

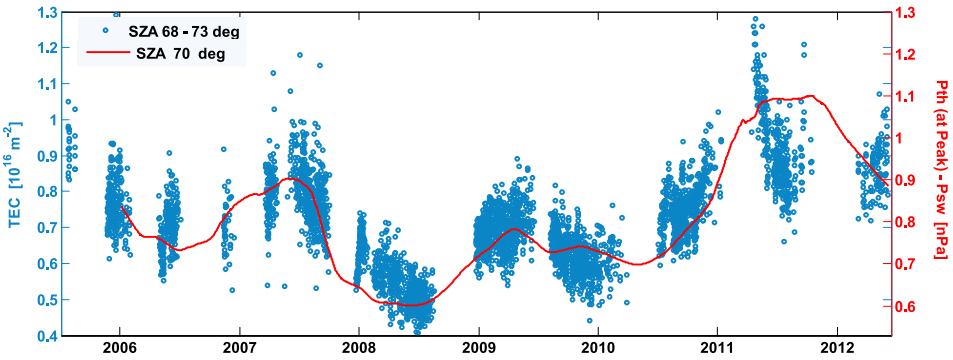

Figure 10. Left *y* axis: TEC of the full ionosphere measured by MARSIS in the subsurface mode (blue dots) over the full solar cycle covered by MARSIS instrument (data from Figure 7). Right *y* axis: Pressure difference between the maximum thermal pressure (red line) from MARSIS AIS mode and the solar wind pressure with solar cycle (data from Figure 9).

hypothetical magnetized ionosphere could be found more easily. The pressure difference is shown in Figure 9c. To help with the discussion, the Mars heliocentric distance and the solar irradiance of 30.5 nm at Mars distance are shown in Figures 9d and 9e, respectively.

If Figures 7 and 9 are compared (Figure 10), the TEC of the full atmosphere follows very closely the behavior of the pressure difference plot (obtained with independent data sets), even at the border between periods B and C where the TEC observations could not be reproduced by the NeMars model with the new empirical modeled scale heights. Figure 10 suggests that the entire Martian plasma system behavior with solar cycle is consistently driven by the relationship between the solar wind dynamic pressure and the maximum thermal pressure of the ionosphere, as the total electron content within the atmosphere closely follows the variation in the difference between the two pressures. Moreover, Figure 10 also indicates the good agreement between two totally independent data sets, such as MARSIS AIS mode and MARSIS subsurface mode data sets. In general, the pressure relationship was weaker when Mars was at a larger distance from the Sun, being the weakest in the year 2008 for all considered SZA. The combination of a very low solar flux plus the farthest orbital distance caused the weakest ionosphere of the solar cycle to compete with the solar wind pressure, which did not change significantly. Evidence of this weak ionosphere has been widely shown in this study with AIS and subsurface MARSIS and radio occultation data sets, and in previous studies such as *Sánchez-Cano et al.* [2015b]. On the other hand, we note that the solar wind dynamic pressure scaled to Mars was not at its absolute minimum, which occurred in 2010 (see Figure 9a). We conclude that during the low solar activity period, the ionosphere may have been in a more continuously magnetized state than in other periods. The induced magnetic field pressure, even if weak, was closer to the ionospheric pressure (which was the weakest of the solar cycle) allowing the field to penetrate to lower altitudes. Therefore, the ionopause could be found at lower altitudes and, as a consequence, the topside ionosphere had the most reduced *H* of the solar cycle. This is confirmed by the lower scale height of Figure 2, as well as by-products of the scale height: the lower density of Figures 3 and 4, the lowest temperatures of Figure 8, and the lowest thermal peak pressure of Figure 9b. Furthermore, this is also confirmed with independent data sets such as the extreme reduction in TEC data given by MARSIS in the subsurface mode (Figure 7) and the radio occultation profiles of Figure 6.

6. Discussion

Since the Sun is the main source of ionization in the Martian upper atmosphere, a different response in the ionization distribution with altitude is expected for the different phases of the solar cycle. Until now, our information has been limited by the amount of data and by the strong planetary coverage restrictions of the radio occultation data sets. Therefore, only now, after over 10 years of Mars Express data, it is possible to analyze the ionospheric response to changes in the solar activity during a solar cycle with the same data set and with an almost complete planetary coverage. This ionospheric reaction can be analyzed from many different points of view. Here we have focused on the neutral scale height since it can be retrieved easily from the Chapman formulation and gives important information of the neutral distribution at ionospheric altitudes. Furthermore, many important by-products can be obtained, inter alia, the TEC, the medium's temperature, or the thermal pressure.

The neutral scale height shows a clear evolution with the solar cycle. While there is almost no variation with the solar zenith angle for the moderate-descending phase and the low solar phases of the solar cycle, the neutral scale height shows large changes with this parameter for the moderate-ascending and high solar activity phases. As a consequence, the neutral and plasma temperatures during the two first periods corroborated previous Mars Express findings: the temperature had virtually no variation with the solar zenith angle. On the other hand, larger temperature changes with solar zenith angle for both neutral and ionized gases are found in the two latest periods. Moreover, similar to the Earth case, the coolest ionosphere and warmest ionosphere were found in the extreme phases of the solar cycle: low and high, respectively. In general terms, if Figures 1 and 8 are compared, both types of derived temperatures from the scale height study follow the solar cycle pattern.

The interaction between the solar wind and the colder Martian plasma can be analyzed as a useful by-product of the neutral scale height. From this scale height, the plasma pressure is easily derived for the peak of the ionosphere, and the maximum thermal pressure of the ionosphere can be estimated, which has a direct dependence on the ionization, created by the solar flux. When the thermal pressure is strong enough to compete with the solar wind pressure, the ionosphere is in normal conditions. However, if this relationship is of the same order of magnitude, the induced magnetic field pressure can have an important role at ionospheric altitudes and reductions in the scale height can be produced. Some evidence of this relationship was observed in the previous work of *Sánchez-Cano et al.* [2015b], where a general density reduction was found for low solar activity, mostly due to a recurrent-induced magnetic field in the ionosphere. Although it is not possible to absolutely confirm that the ionosphere was in this state during the low solar activity period, there is clear evidence that at least, this was the time when the solar and thermal pressures had the weaker relationship. Therefore, it is possible to state that during the low solar cycle phase, the ionosphere of Mars had the highest probability to be in a magnetized state and is reflected in the scale height reductions observed in several data sets from Mars Express, such as MARSIS AIS, MARSIS subsurface, or radio occultation. As can be extrapolated from Figure 10, the full ionosphere TEC measured by MARSIS in the subsurface mode closely follows the shape of the daily pressures relationship.

The neutral scale height is an important parameter to describe the behavior of the density distribution in the ionosphere, which, in turn, can be a dynamic indicator of the solar wind-Martian plasma interaction, as well as of the temperature of the medium. The period of low solar activity deserves a significant mention. Here a major density reduction was found in the ionospheric topside mostly due to the reduction in the EUV. Furthermore, the extreme reduction in solar X-ray flux could have caused an almost permanent absence of the secondary layer, as observed by MaRS instrument. Despite the limited observations, the analysis of the TEC daily evolution in Figure 7 and the pressure relationship between dynamic solar wind pressure and maximum thermal pressure (calculated from AIS data set) in Figure 10 show that this scenario is totally realistic and consistent with MaRS, as the predicted TEC by the model and the MARSIS subsurface observations agree with this hypothesis. Additionally, this is somehow confirmed by the recent work carried out by *Ao et al.* [2015], which has provided the first demonstration of cross-link occultation density profiles between two different spacecraft, the first time that this happens at a planet other than Earth. The series of three cross-link occultation experiments were acquired between the Mars Odyssey and Mars Reconnaissance Orbiter spacecraft in September 2007 with solar zenith angles between 40 and 53°, much lower than the ones that we show in this study. The three profiles that they show correspond to the transition time between periods A and B in our study. Therefore, any comparison should be treated like profiles with transition characteristics between both periods. As observed in *Ao et al.* [2015], the secondary layer totally disappeared in one of the profiles (the one which has a more reduced topside).

The work presented in this paper is totally consistent with the general interaction of the solar wind with non-magnetic bodies. At Venus, as at Mars, the solar wind interaction with the planet is strongly dependent on the phase of the solar cycle [e.g., *Alexander and Russell*, 1985; *Zhang et al.*, 1990; *Russell et al.*, 2006; *Bertucci et al.*, 2011]. At solar minimum, the Venusian bow shock and ionopause are found to be closer to the planet than at solar maximum. The dayside ionosphere is smaller in altitude, and its ionopause density gradient is not so clearly defined during solar minimum whereas the density gradient is rather sharp at solar maximum [*Knudsen et al.*, 1987]. Moreover, during solar minimum, there is a higher probability that the ionosphere becomes magnetized [e.g., *Russell et al.*, 2006] like at Mars.

A thorough survey of the whole MaRS observations for both layers and their dependence on solar flux is currently under development. Future studies will expand this work by including more recent data during the

high solar activity phase, as well as numerical simulations in order to better understand the global ionospheric response during a complete solar cycle.

7. Conclusions

We here list the main conclusions derived from this study.

1. Multiple data sets have been utilized in this study, such as the Mars Express MARSIS radar in its Active Ionospheric Sounding (AIS) mode, the Mars Express MARSIS radar total electron content (TEC) derived from the subsurface operational mode, the Mars Express MaRS instrument, and the solar wind moments derived from Earth-based satellites: TIME-SEE, ACE, and OMNI data set.
2. The neutral scale height behavior of the main layer of the ionosphere of Mars in the photochemical region has different characteristics in each phase of the solar cycle 23/24.
3. During the low solar activity period, a major density reduction was found in the ionospheric topside mostly due to the reduction in the EUV flux. The largest topside densities, however, are found in the period of high solar activity, in accordance with the EUV intensification.
4. For the moderate-descending low solar activity phases of the solar cycle (A and B), the neutral scale height does not show any pronounced variation with the solar zenith angle. Therefore, neutral and plasma temperatures and plasma pressure have a similar behavior with respect to solar illumination.
5. For the moderate-ascending and high solar activity phases of the solar cycle (C and D), a larger dependence on the solar zenith angle is found, and therefore, neutral and plasma temperatures and plasma pressure have a similar behavior.
6. The main peak density is, on average, 7% statistically significant lower in low solar activity phase than in the other three periods.
7. The main peak altitude is, on average, an 8% statistically significant lower (13 km in absolute difference) in high solar activity period than in the other three phases.
8. The extreme reduction in X-rays solar flux during the period of low solar activity produced a significant reduction of the bottomside of the main layer, as well as an almost permanent secondary layer absence.
9. When the relationship between the solar dynamic pressure at Mars and the maximum thermal pressure of the ionosphere along the solar cycle was at its weakest, there was a larger probability of having the ionosphere in a more magnetized state. This is manifested in a more reduced topside density profile.
10. The total ionospheric TEC shape follows the nature of the pressure relationship between the solar wind and the maximum thermal pressures (Figure 10).

Acknowledgments

B.S.-C., M.L., and S.E.M. acknowledge support through STFC grant ST/K001000/1 and B.E.S.H. from the STFC Ph.D. studentship ST/K502121/1. B.S.-C. acknowledges a scientific stay at ESA-ESTEC by ESTEC Faculty support funding. The Mars Express MARSIS AIS data were downloaded from the European Space Agency Planetary Science Archive (http://www.rssd.esa.int/psa), the solar flux data from the NOAA service (ftp://ftp.swpc.noaa.gov/pub/warehouse/), the TIMED-SEE data from the University of Colorado's website (http://lasp.colorado.edu/lisird/index.html), the ACE solar data from the ACE Science Center (http://www.srl.caltech.edu/ACE/ASC/index.html), and the OMNI data from the NASA space physics data facility (ftp://spdf.gsfc.nasa.gov/pub/data/omni/low_res_omni/). Data from MARSIS subsurface are from *Cartacci et al.* [2013] algorithm. Mars Express MaRS instrument data are from the Rheinisches Institut für Umweltforschung an der Universität zu Köln (Germany) and can be requested from martin.paetzold@uni-koeln.de. The German part of the Mars Express Radio Science experiment (MaRS) is funded by the Bundesministerium für Wirtschaft BMWi, Berlin, via the German Space Agency DLR, Bonn, under grants 50QM1004, 50QM1401 (both RIU-PF), and 50QM1002 (UniBw). All data used in this study will be available on request to the author [bscmdr1@leicester.ac.uk].

References

Acuña, M. H., et al. (1999), Global distribution of crustal magnetization discovered by the Mars Global Surveyor MAG/ER Experiment, *Science*, *28*(5415), 790–793, doi:10.1126/science.284.5415.790.

Akalin, F., D. D. Morgan, D. A. Gurnett, D. L. Kirchner, D. A. Brain, R. Modolo, M. H. Acuna, and J. R. Espley (2010), Dayside induced magnetic field in the ionosphere of Mars, *Icarus*, *206*, 104–111, doi:10.1016/j.icarus.2009.03.021.

Alexander, C. J., and C. T. Russell (1985), Solar cycle dependence of the location of the Venus bow shock, *Geophys. Res. Lett.*, *12*(6), 369–371.

Ao, C. O., C. D. Edwards Jr., D. S. Kahan, X. Pi, S. W. Asmar, and A. J. Mannucci (2015), A first demonstration of Mars crosslink occultation measurements, *Radio Sci.*, *50*, 997–1007, doi:10.1002/2015RS005750.

Bertucci, C., C. Mazelle, and M. H. Acuña (2005), Interaction of the solar wind with Mars from Mars Global Surveyor MAG/ER observations, *J. Atmos. Sol. Terr. Phys.*, *67*, 1797–1808, doi:10.1016/j.jastp.2005.04.007.

Bertucci, C., F. Duru, N. Edberg, M. Fraenz, C. Martinecz, K. Szego, and O. Vaisberg (2011), The induced magnetospheres of Mars, Venus, and Titan, *Space Sci. Rev.*, *162*, 113–171, doi:10.1007/s11214-011-9845-1.

Bertucci, C., D. C. Hamilton, W. S. Kurth, G. Hospodarsky, D. Mitchell, N. Sergis, N. J. T. Edberg, and M. K. Dougherty (2015), Titan's interaction with the supersonic solar wind, *Geophys. Res. Lett.*, *42*, 193–200, doi:10.1002/2014GL062106.

Bougher, S., et al. (2015b), Early MAVEN deep dip campaign reveals thermosphere and ionosphere variability, *Science*, *350*(6261), doi:10.1126/science.aad0459.

Bougher, S. W., D. Pawlowski, J. M. Bell, S. Nelli, T. McDunn, J. R. Murphy, M. Chizek, and A. Ridley (2015a), Mars Global Ionosphere-Thermosphere Model (MGITM): Solar cycle, seasonal, and diurnal variations of the Mars upper atmosphere, *J. Geophys. Res. Planets*, *120*, 311–342, doi:10.1002/2014JE004715.

Cain, J. C., B. B. Ferguson, and D. Mozzoni (2003), An $n = 90$ internal potential function of the Martian crustal magnetic field, *J. Geophys. Res.*, *108*(E2), 5008, doi:10.1029/2000JE001487.

Cartacci, M., E. Amata, A. Cicchetti, R. Noschese, S. Giuppi, B. Langlais, A. Frigeri, R. Orosei, and G. Picardi (2013), Mars ionosphere total electron content analysis from MARSIS subsurface data, *Icarus*, *223*(1), 423–437, doi:10.1016/j.icarus.2012.12.011.

Chapman, S. (1931a), Absorption and dissociative or ionizing effects of monochromatic radiation in an atmosphere on a rotating earth, *Proc. Phys. Soc. Lond.*, *43*, 26–45.

Chapman, S. (1931b), Absorption and dissociative or ionizing effect of monochromatic radiation in an atmosphere on a rotating Earth. Part II. Grazing incidence, *Proc. Phys. Soc. Lond.*, *43*, 483–501.

Chicarro, A., P. Martin, and R. Traunter (2004), Mars Express: A European mission to the red planet, European Space Agency Publication Division, SP-1240, pp. 3–16, Noordwijk, Netherlands.
Cravens, T. E. (1997), *Physics of Solar System Plasmas*, Cambridge Univ. Press, Cambridge, U. K.
Cui, J., M. Galand, S. J. Zhang, E. Vigren, and H. Zou (2015), The electron thermal structure in the dayside Martian ionosphere implied by the MGS radio occultation data, *J. Geophys. Res. Planets*, *120*, 278–286, doi:10.1002/2014JE004726.
Dubinin, E., et al. (2008), Structure and dynamics of the solar wind/ionosphere interface on Mars: MEXASPERA-3 and MEX-MARSIS observations, *Geophys. Res. Lett.*, *35*, L11103, doi:10.1029/2008GL033730.
Edberg, N. J. T., M. Lester, S. W. H. Cowley, and A. I. Eriksson (2008), Statistical analysis of the location of the Martian magnetic pileup boundary and bow shock and the influence of crustal magnetic fields, *J. Geophys. Res.*, *113*, A08206, doi:10.1029/2008JA013096.
Edberg, N. J. T., et al. (2009), Simultaneous measurements of the Martian plasma boundaries by Rosetta and Mars Express, *Planet. Space Sci.*, *57*(8–9), 1085–1096, doi:10.1016/j.pss.2008.10.016.
Ergun, R. E., M. W. Morooka, L. A. Andersson, C. M. Fowler, G. T. Delory, D. J. Andrews, A. I. Eriksson, T. McEnulty, and B. M. Jakosky (2015), Dayside electron temperature and density profiles at Mars: First results from the MAVEN Langmuir probe and waves instrument, *Geophys. Res. Lett.*, *42*, 8846–8853, doi:10.1002/2015GL065280.
Forbes, J. M., F. G. Lemoine, S. L. Bruinsma, M. D. Smith, and X. Zhang (2008), Solar flux variability of Mars' exosphere densities and temperatures, *Geophys. Res. Lett.*, *35*, L01201, doi:10.1029/2007GL031904.
Forget, F., F. Montmessin, J.-L. Bertaux, F. González-Galindo, S. Lebonnois, E. Quémerais, A. Reberac, E. Dimarells, and M. A. López-Valverde (2009), Density and temperatures of the upper Martian atmosphere measured by stellar occultations with Mars Express SPICAM, *J. Geophys. Res.*, *114*, E01004, doi:10.1029/2008JE003086.
Frahm, R. A., et al. (2006), Carbon dioxide photoelectron peaks at Mars, *Icarus*, *182*, 371–382, doi:10.1016/j.icarus.2006.01.014.
Girazian, Z., and P. Withers (2013), The dependence of peak electron density in the ionosphere of Mars on solar irradiance, *Geophys. Res. Lett.*, *40*, 1960–1964, doi:10.1002/grl.50344.
González-Galindo, F., J.-Y. Chaufray, M. A. Lopez-Valverde, G. Gilli, F. Forget, F. Leblanc, R. Modolo, S. Hess, and M. Yagi (2013), Three-dimensional Martian ionosphere model: I. The photochemical ionosphere below 180 km, *J. Geophys. Res. Planets*, *118*, 2105–2123, doi:10.1002/jgre.20150.
Gurnett, D. A., et al. (2005), Radar soundings of the ionosphere of Mars, *Science*, *310*, 1999–1933, doi:10.1126/science.1121868.
Gurnett, D. A., et al. (2008), An overview of radar soundings of the Martian ionosphere from the Mars Express spacecraft, *Adv. Space Res.*, *41*, 1335–1346, doi:10.1016/j.asr.2007.01.062.
Hanson, W. B., and G. P. Mantas (1988), Viking electron temperature measurements: Evidence for a magnetic field in the Martian ionosphere, *J. Geophys. Res.*, *93*(A7), 7538–7544.
Hanson, W. B., S. Sanatani, and D. R. Zuccaro (1977), The Martian ionosphere as observed by the Viking retarding potential analyzers, *J. Geophys. Res.*, *82*, 4351–4363.
Imber, S. M., S. E. Milan, and M. Lester (2013), Solar cycle variations in polar cap area measured by the superDARN radars, *J. Geophys. Res. Space Physics*, *118*, 6188–6196, doi:10.1002/jgra.50509.
Keating, G. M., et al. (1998), The structure of the upper atmosphere of Mars. In situ accelerometer measurements from Mars Global Surveyor, *Science*, *279*, 1672–1676.
Knudsen, W. C., et al. (1987), Solar cycle changes in the ionization sources of the nightside Venus ionosphere, *J. Geophys. Res.*, *92*, 13,391–13,398.
Leblanc, F., J. Y. Chaufray, J. Lilensten, O. Witasse, and J. L. Bertaux (2006), Martian dayglow as seen by the SPICAM UV spectrograph on Mars Express, *J. Geophys. Res.*, *111*, E09S11, doi:10.1029/2005JE002664.
Matta, M., M. Mendillo, P. Withers, and D. Morgan (2015), Interpreting Mars ionospheric anomalies over crustal magnetic field regions using a 2-D ionospheric model, *J. Geophys. Res. Space Physics*, *120*, 766–777, doi:10.1002/2014JA020721.
Mendillo, M., P. Withers, D. Hinson, H. Rishbeth, and B. Reinisch (2006), Effects of solar flares on the ionosphere of Mars, *Science*, *311*, 1135–1138, doi:10.1126/science.1122099.
Morel, L., O. Witasse, R. Warnant, J.-C. Cerisier, P.-L. Blelly, and J. Lilensten (2004), Diagnostic of the dayside ionosphere of Mars using the total electron content measurement by the NEIGE/Netlander experiment: An assessment study, *Planet. Space Sci.*, *52*(7), 603–611, doi:10.1016/j.pss.2003.12.007.
Morgan, D. D., O. Witasse, E. Nielsen, D. A. Gurnett, F. Duru, and D. L. Kirchner (2013), The processing of electron density profiles from the Mars Express MARSIS topside sounder, *Radio Sci.*, *48*, 197–207, doi:10.1002/rds.20023.
Mouginot, J., W. Kofman, A. Safaeinili, and A. Herique (2008), Correction of the ionospheric distortion on the MARSIS surface sounding echoes, *Planet. Space Sci.*, *56*, 917–926, doi:10.1016/j.pss.2008.01.010.
Nicholson, W. P., G. Gronoff, J. Lilensten, A. D. Aylward, and C. Simon (2009), A fast computation of the secondary ion production in the ionosphere of Mars, *Mon. Not. R. Astron. Soc.*, *400*, 369–382, doi:10.1111/j.1365-2966.2009.15463.x.
Opgenoorth, H. J., D. J. Andrews, M. Franz, M. Lester, N. J. T. Edberg, D. Morgan, F. Duru, O. Witasse, and A. O. Williams (2013), Mars ionospheric response to solar wind variability, *J. Geophys. Res. Space Physics*, *118*, 6558–6587, doi:10.1002/jgra.50537.
Orosei, R., et al. (2014), Mars Advanced Radar for Subsurface and Ionospheric Sounding (MARSIS) after nine years of operation: A summary, *Planet. Space Sci.*, doi:10.1016/j.pss.2014.07.010.
Pätzold, M., et al. (2009), MaRS: Mars express radio science experiment, in *Mars Express: The Scientific Payload*, vol. 1291, edited by A. Wilson and A. Chicarro, pp. 217–248, ESA Spec. Publ., Noordwijk, Netherlands.
Peter, K., et al. (2014), The dayside ionospheres of Mars and Venus: Comparing a one-dimensional photochemical model with MaRS (Mars Express) and VeRa (Venus Express) observations, *Icarus*, *233*, 66–82, doi:10.1016/j.icarus.2014.01.028.
Picardi, G., et al. (2004), Mars Express: A European mission to the red planet, MARSIS: Mars Advanced Radar for Subsurface and Ionosphere Sounding, Eur. Space Agency Publ. Div., SP-1240, pp. 51-70, Noordwijk, Netherlands.
Rawer, K. (1993), *Wave Propagation in the Ionosphere*, Kluwer Acad. Publ., Dordrecht, Netherlands.
Rees, M. H. (1989), *Physics and Chemistry of the Upper Atmosphere*, 98 pp., Cambridge Univ. Press, Cambridge, U. K.
Russell, C. T., and O. Vaisberg (1983), The interaction of the solar wind with Venus, in *Venus*, edited by D. M. Hunten et al., pp. 873–940, Univ. of Ariz. Press, Tuscon.
Russell, C. T., J. G. Luhmann, and R. J. Strangeway (2006), The solar wind interaction with Venus through the eyes of the Pioneer Venus Orbiter, *Planet. Space Sci.*, *54*, 1482–1495, doi:10.1016/j.pss.2006.04.025.
Safaeinili, A., W. Kofman, J. Mouginot, Y. Gim, A. Herique, A. B. Ivanov, J. Plaut, and G. Picardi (2007), Estimation of the total electron content of the Martian ionosphere using radar sounder surface echoes, *Geophys. Res. Lett.*, *34*, L23204, doi:10.1029/2007GL032154.
Sánchez-Cano, B., S. M. Radicella, M. Herraiz, O. Witasse, and G. Rodríguez – Caderot (2013), NeMars: An empirical model of the Martian dayside ionosphere based on Mars Express MARSIS data, *Icarus*, *225*, 236–247, doi:10.1016/j.icarus.2013.03.021.

Sánchez-Cano, B., et al. (2015a), Total electron content in the Martian atmosphere: A critical assessment of the Mars Express MARSIS datasets, *J. Geophys. Res. Space Physics*, *120*, 2166–2182, doi:10.1002/2014JA020630.

Sánchez-Cano, B., M. Lester, O. Witasse, S. E. Milan, B. E. S. Hall, P.-L. Blelly, S. M. Radicella, and D. D. Morgan (2015b), Evidence of scale height variations in the Martian ionosphere over the solar cycle, *J. Geophys. Res. Space Physics*, *120*, 10,913–10,925, doi:10.1002/2015JA021949.

Sánchez-Cano, B., O. Witasse, M. Herraiz, S. M. Radicella, J. Bauer, P.-L. Blelly, and G. Rodríguez-Caderot (2012), Retrieval of ionospheric profiles from the Mars Express MARSIS experiment data and comparison with radio-occultation data, *Geosci. Instrum., Methods Data Syst.*, *1*, 77–84, doi:10.5194/gi-1-77-2012.

Schunk, R., and A. F. Nagy (2009), *Ionospheres: Physics, Plasma Physics, and Chemistry*, Cambridge Univ. Press, Cambridge, U. K.

Shinagawa, H., and T. E. Cravens (1989), A one-dimensional multispecies magnetohydrodynamic model of the dayside ionosphere of Mars, *J. Geophys. Res.*, *94*(A6), 6506–6516, doi:10.1029/JA094iA06p06506.

Shinagawa, H., and T. E. Cravens (1992), The ionospheric effects of a weak intrinsic magnetic field at Mars, *J. Geophys. Res.*, *97*(E1), 1027–1035, doi:10.1029/91JE02720.

Solomon, S. C., T. N. Woods, L. V. Didkovsky, J. T. Emmert, and L. Qian (2010), Anomalously low solar extreme-ultraviolet irradiance and thermospheric density during solar minimum, *Geophys. Res. Lett.*, *37*, L16103, doi:10.1029/2010GL044468.

Stewart, A. I. (1972), Mariner 6 and 7 ultraviolet spectrometer experiment: Implications of CO2+, CO and O airglow, *J. Geophys. Res.*, *77*, 54–68.

Stiepen, A., J.-C. Gerard, S. Bougher, F. Montmessin, B. Hubert, and J.-L. Bertaux (2015), Mars thermospheric scale height: CO Cameron and CO_2 + dayglow observations from Mars Express, *Icarus*, *245*, 295–305, doi:10.1016/j.icarus.2014.09.051.

Wang, J.-S., and E. Nielsen (2004), Evidence for topographic effects on the Martian ionosphere, *Planet. Space Sci.*, *52*(9), 881–886, doi:10.1016/j.pss.2004.01.008.

Whitten, R. C., and L. Colin (1974), The ionospheres of Mars and Venus, *Rev. Geophys. Space Phys.*, *12*(2), 155–192.

Witasse, O. (2000), Modélisation des Ionosphères planétaires et de leur Rayonnement: La Terre et Mars, PhD thesis, Laboratoire de Planétologie de Grenoble.

Witasse, O., T. Cravens, M. Mendillo, J. Moses, A. Kliore, F. Nagy, and T. Breus (2008), Solar system ionospheres, *Space Sci. Rev.*, *139*, 235–265, doi:10.1007/s11214-008-9395-3.

Withers, P. (2009), A review of observed variability in the dayside ionosphere of Mars, *Adv. Space Res.*, *44*, 277–307, doi:10.1016/j.asr.2009.04.027.

Withers, P., and R. Pratt (2013), An observational study of the response of the upper atmosphere of Mars to lower atmospheric dust storms, *Icarus*, *225*, 378–389, doi:10.1016/j.icarus.2013.02.032.

Withers, P., S. W. Bougher, and G. M. Keating (2003), The effects of topographically-controlled thermal tides in the Martian upper atmosphere as seen by the MGS accelerometer, *Icarus*, *164*(2003), 14–32, doi:10.1016/S0019-1035(03)00135-0.

Withers, P., et al. (2012a), A clear view of the multifaceted dayside ionosphere of Mars, *Geophys. Res. Lett.*, *39*, L18202, doi:10.1029/2012GL053193.

Withers, P., M. O. Fillingim, R. J. Lillis, B. Häusler, D. P. Hinson, G. L. Tyler, M. Pätzold, K. Peter, S. Tellmann, and O. Witasse (2012b), Observations of the nightside ionosphere of Mars by the Mars Express Radio Science Experiment (MaRS), *J. Geophys. Res.*, *117*, A12307, doi:10.1029/2012JA018185.

Withers, P., D. D. Morgan, and D. A. Gurnett (2014), Variations in peak electron densities in the ionosphere of Mars over a full solar cycle, *Icarus*, doi:10.1016/j.icarus.2014.08.008.

Zhang, M. H. G., and J. G. Luhmann (1992), Comparisons of peak ionosphere pressures at Mars and Venus with incident solar wind dynamic pressure, *J. Geophys. Res.*, *97*(E1), 1017–1025.

Zhang, T.-L., J. G. Luhmann, and C. T. Russell (1990), The solar cycle dependence of the location and shape of the Venus bow shock, *J. Geophys. Res.*, *95*, 14,961–14,967.

Zou, H., R. J. Lillis, J. S. Wang, and E. Nielsen (2011), Determination of seasonal variations in the Martian neutral atmosphere from observations of ionospheric peak height, *J. Geophys. Res.*, *116*, E09004, doi:10.1029/2011JE003833.